Journal of Thermal Analysis and Calorimetry (2023) 148:10595–10644
https://doi.org/10.1007/s10973-023-12438-0

A comprehensive review of computational fluid dynamics simulation studies in phase change materials: applications, materials, and geometries

A. Mohammadian Soodmand[1] · B. Azimi[1] · S. Nejatbakhsh[1] · H. Pourpasha[1] · M. Ebrahimi Farshchi[1] · H. Aghdasinia[1] · M. Mohammadpourfard[3] · S. Zeinali Heris[1,2]

Received: 28 February 2023 / Accepted: 22 July 2023 / Published online: 11 August 2023

Abstract

Thermal energy storage systems (TESS) have emerged as significant global concerns in the design and optimization of devices and processes aimed at maximizing energy utilization, minimizing energy loss, and reducing dependence on fossil fuel energy for both environmental and economic reasons. Phase change materials (PCMs) are widely recognized as promising candidates due to their high latent heat storage (LHS) capacity. This review thoroughly evaluates the computational fluid dynamics (CFD) studies conducted in various sections, encompassing materials, modeling, simulation, as well as the results, advantages, and disadvantages of these works. The study is organized into three distinct sections. The first section discusses the applications of PCMs in various areas, including lithium-ion batteries, solar applications, building applications, electronics, and heating and cooling systems. The second section provides a comprehensive summary of cylindrical, rectangular, spherical, arbitrary shapes, and packed-bed geometries employed in TESS. The third section investigates the different types of materials used as PCMs. Based on the findings of this study, it can be concluded that industrial applications of hybrid nanocomposites incorporating PCMs in different geometries pose challenges, particularly in three-dimensional (3D) settings, where instability becomes a significant concern. Hence, further research and investigation are necessary to address these challenges adequately. In conclusion, this study serves as a reference review for future research endeavors in the field of simulating various PCMs in different geometries and applications. It provides valuable insights into the current state of knowledge, highlights potential areas for improvement, and offers guidance for advancing simulation techniques related to PCMs.

Keywords Phase change materials (PCMs) · Thermal energy storage system (TESS) · CFD simulation · Geometry

Abbreviations

ASHRAE	American Society of Heating, Refrigerating and Air-Conditioning Engineers
CFD	Computational fluid dynamic
CPCM	Composite phase change material
CPU	Central processing unit
CVFD	Control-volume finite difference
e-NTU	Effectiveness-number of transfer units
EG	Expended graphite
ESS	Energy storage systems
FDM	Finite difference method
FEM	Finite element method
FVM	Finite volume method
HTC	Heat transfer coefficient
HTF	Heat transfer fluid
HTR	Heat transfer rate
HTTD	Heat transfer temperature difference
HVAC	Heating, ventilation, and air conditioning
LHS	Latent heat storage
LTES	Latent thermal energy storage
NEPCM	Nano-enhanced PCM
NP	Nano particle
PCMs	Phase change materials
PW	Paraffin wax
RNG	Renormalization group

✉ S. Zeinali Heris
s.zeinali@tabrizu.ac.ir

[1] Faculty of Chemical and Petroleum Engineering, University of Tabriz, Tabriz, Iran

[2] Xi'an University of Science and Technology, No. 58, Middle Section of Yanta Road, Xi'an 710054, Shaanxi, China

[3] Department of Energy Systems Engineering, Izmir Institute of Technology, Izmir, Turkey

SE	Solar energy
SEM	Scanning electron microscopy
SHS	Sensible heat storage
SST	Shear stress transport
TCR	Thermal contact resistance
TESS	Thermal energy storage system
TMS	Thermal management system
TS	Thermal storage
TSS	Thermal storage system
UDF	User-defined function
2D	Two-dimensional
3D	Three-dimensional

List of symbols

$A(\beta)$	Porosity function
A_{mush}	Mushy zone constant
C_{P}	Specific heat
H	Specific enthalpy
h	Enthalpy
h_{sl}	Latent heat
ΔH	Sum of latent heat
k_{l}	Thermal conductivity of the liquid phase
k_s	Thermal conductivity of the solid phase
L	Latent heat of freezing of the material
l	Specific length
n	Normal vector at the interface
T	Temperature
T_{s}	Temperature of solid
T_{l}	Temperature of liquid
Ra	Rayleigh number
S	Momentum source term
T	Temperature
$\overline{v}$	Fluid normal velocity
ρ	Density
β	Volumetric expansion coefficient

Introduction

It is widely acknowledged that the excessive utilization of fossil fuels, resulting in increased greenhouse gas emissions, particularly CO_2, has significantly contributed to anthropogenic climate change and global warming [1, 2]. Currently, fossil fuels still account for 80% of the global energy demand, and this reliance is projected to persist in the coming decades, despite advancements in renewable energy sources [3]. However, the combination of escalating energy needs, diminishing availability of traditional energy resources, and environmental concerns associated with fossil fuel usage has prompted a substantial transition toward renewable energy options like hydropower, solar power, wind power, geothermal energy, and biomass over the past twenty years [4]. In order to mitigate greenhouse gas emissions, it is imperative to both increase the proportion of renewable energy in overall energy consumption and enhance energy efficiency [5]. Additionally, it is vital to reduce the tendency for using fossil fuels due to the depletion of fossil resources [6]. This approach is crucial for curbing the volume of greenhouse gas emissions. Furthermore, the depletion of fossil fuel reserves necessitates a reduction in their reliance [4]. For instance, global initiatives to decrease CO_2 emissions and address the decline of oil resources have led to the emergence of electric vehicles and hybrid electric vehicles as viable alternatives to combustion engine-powered vehicles [7].

Considering the declining trend and limited availability of conventional energy resources, as well as the environmental problems associated with climate change and air pollution, there is a growing need to shift toward green and renewable energy resources, such as wind, solar, hydropower, geothermal, and biomass. These types of energy sources have strong potential for utilization in industrial and domestic heating applications [8]. However, it should be noted that many renewable energy sources, including solar and wind, are inherently intermittent, which necessitates the efficient storage of energy to bridge the gap between demand and supply [9]. Storing thermal energy from sustainable sources (e.g., solar) or recovering waste heat in industrial processes is critical in a world confronted with rising energy demand and climate changes [10]. Despite the aforementioned properties of sustainable energy, energy extraction from these sources faces stability limitations such as reliance on weather conditions, space, and time. A TESS serves as a useful tool for reducing supply–demand imbalances and achieving continuous, dispatchable electricity output due to the intermittent and unstable nature of these energy sources.

TESS has gained significant interest worldwide in the fields of renewable energy and other high-temperature applications, including waste heat recovery and utilization [11, 12]. TESS refers to a collection of technologies that store excessive energy in the form of heat and utilize it either directly or indirectly through energy conversion processes when needed. This technique is essential for balancing energy supply and demand, particularly in applications involving time-varying energy sources such as solar and wind. Numerous investigations have been conducted to design thermal management systems (TMSs) using traditional approaches such as air cooling [13, 14] and heat pipe cooling [15]. Latent thermal energy storage (LTES), which has a large energy storage (ES) capacity and operates with almost isothermal properties, has received significant attention in various engineering sectors to address changes in thermal energy demand. PCMs are suitable choices for use in LTES systems due to their high energy storage density, nearly isothermal solid–liquid phase change behavior, and the variety of forms they come in. This makes them

applicable for electronic device cooling [16, 17], thermal storage (TS) in buildings [18], and refrigeration and cooling [19]. Consequently, the development of new energy storage systems (ESS) based on PCMs is considered an approach for storing generated energy to be used when needed, as they can absorb and release energy at a constant temperature during phase transition. Organic PCMs with high latent heat of fusion, such as paraffin wax (PW), enable the design of compact TESS units with large capabilities [20]. However, to obtain these benefits, appropriate design approaches that consider the energy losses occurring within the PCM are necessary. The generally low thermal conductivities of many organic PCMs can affect the melting and solidification times, as well as the charging and discharging times of the storage system, which is one of the fundamental disadvantages [21]. The appropriate PCM is one that is chemically inert, stable, and nonflammable. To improve heat transfer efficiency throughout the phase change process, it must maintain its solid state during phase transition and exhibit a considerable latent heat of phase change, along with a high thermal conductivity. Consequently, enhancing the thermal conductivity of PCMs has become a challenging issue in LTES systems, especially for high-power devices. Multiple techniques have been investigated and performed by many researchers, such as adding fins, ribs, and applying surface waviness to improve the heat transfer rate (HTR) of PCMs [22]. The placement of highly conductive materials like metal filters, foams, and nanoparticles can be helpful. The PCM containment should be thermally stable and possess appropriate mechanical strength. Additionally, it should provide sufficient surface area for heat transfer [23]. An LTES system consists of the following components: (a) a PCM with the appropriate melting-solidification point for the intended temperature range, (b) a PCM container, and (c) the use of a heat exchanger to transfer heat from the heat source into the PCM and subsequently from the PCM to the heat sink [24].

Analytical methods to solve problems involving phase change phenomena are difficult to achieve due to the nonlinear phase front interface, which is controlled by variations in latent heat at the boundary, especially when dealing with complex 3D geometries [25, 26]. Therefore, numerical methods have been widely used in recent years to simulate phase change problems. CFD has proven to be a valuable tool in solving solidification and melting problems with minimal time and effort. Through CFD simulations, it is possible to model and simulate thermal storage systems (TSS) consisting of PCMs and study optimal geometrical configurations, as well as various conventional and novel-laboratory synthesized PCMs for different applications such as lithium-ion batteries, solar energy (SE), building energy-saving systems, electronic devices, and heating–cooling systems. Temperature-based and enthalpy-based methods are the two main approaches used to numerically model phase change processes. The energy equations for the solid and liquid phases are solved separately in the temperature-based approach, which explicitly tracks the interface between the phases. Temperature remains the only dependent variable. Equation (1) expresses the temperature-based formulation.

$$\frac{\partial T_s}{\partial n}k_s = \frac{\partial T_l}{\partial n}k_l + \rho L k v_n \tag{1}$$

T_s and T_l denote the temperatures of the solid and liquid phases, respectively. The terms "k_s" and "k_l" refer to the thermal conductivity of the solid and liquid phases, respectively. At the interface, n is the unit normal vector, and ν_n contributes the normal component of velocity. L indicates the material's latent heat of freezing. The enthalpy method involves formulations with a mushy zone when the liquid and the solid phases are present simultaneously and no explicit condition is expected in this method, which leads to solving the problems in a much easier way [27, 28]. Equation (2) describes the general formulation of the enthalpy method [29].

$$\frac{\partial \rho H}{\partial t} + \nabla.(\rho \bar{v} H) = \nabla.(k \Delta T) + S \tag{2}$$

where T and k are referred to as temperature and the thermal conductivity of the PCM, respectively, ρ is the PCM's density, $\bar{v}$ is the fluid normal velocity, H is the specific enthalpy, and S donates the source term [30].

And H can be defined as Eq. (3).

$$H = h + \Delta H \tag{3}$$

where h can be expressed by Eq. (4).

$$h = h_{ref} + \int_{T_{ref}}^{T} C_p \mathrm{d}T \tag{4}$$

In Eq. (4), h_{ref} is the reference enthalpy at T_{ref}, C_p is the specific heat, and ΔH is the sum of latent heat. Latent heat content can range from zero (for solids) to L (for liquid).

$$\Delta H = \beta L \tag{5}$$

The liquid fraction (β) can be expressed using the following relationships:

$$\beta = \begin{cases} 0 & \text{if } T < T_s \\ \frac{T - T_s}{T_l - T_s} & \text{if } T_s < T < T_l \\ 1 & \text{if } T > T_l \end{cases} \tag{6}$$

The source term S in the momentum equation, Eq. (7), is given by:

$$S = -A(\beta)V \tag{7}$$

where $A(\beta)$ is the "porosity function" defined by Brent et al. [31], as shown in Eq. (8). In the momentum equation, the source term is used to characterize the flow in the porous medium. It must be zero in the liquid phase to allow for free motion, but it must be significant in the solid phase to drive the velocity values toward near-zero values.

$$A(\beta) = \frac{A_{\text{mush}}(1-\beta)^2}{\beta^2 + \varepsilon} \tag{8}$$

where ε is a computational constant used to prevent zero and A_{mush} is the mushy zone constant.

This study is structured into three primary sections, each focusing on distinct aspects of thermal management systems (TMS). The first section comprehensively explores the novel applications of TMS in various domains, including building compartments, lithium-ion batteries, solar energy systems, electronic devices, as well as heating and cooling systems. It delves into the specificities of TMS implementation and its impact in these areas. The second section centers on the investigation of different geometrical structures employed in TMS. It covers a range of geometries, including cylindrical, rectangular, spherical, random, and packed-bed configurations. Each structure is analyzed in terms of its thermal behavior and efficiency in facilitating heat transfer processes. The third section provides an in-depth examination of pure and modified types of materials used as PCMs within TMS applications. These materials are thoroughly studied and evaluated, considering their thermal properties and performance in energy storage and release. The section highlights both the simulation procedures employed and the corresponding findings obtained from each study. Throughout all three sections, particular attention is given to discussing the simulation methodologies used and the key findings derived from the investigations. Moreover, the challenges and debates surrounding TMS in each specific domain are carefully synthesized and summarized in the conclusion of each section. What sets this review apart from other documents is its focus on the utilization of CFD approaches in novel applications, including TESS in lithium-ion batteries and electronic devices. Additionally, the review examines complex geometries such as packed beds and porous media, as well as numerical investigations of advanced additive and composite materials that are not specifically reviewed by other studies [26, 32, 33]. Through critical discussions, practical gaps and advances in these areas are identified. This comprehensive analysis aims to offer researchers a well-rounded perspective and valuable insights for further exploration and advancement within the field of TMS.

Numerical case studies of PCM

Industrial and commercial applications of PCMs

Energy-saving strategies and TESS are applied in a wide range of applications and engineering fields, including lithium-ion batteries, building compartments, electronic devices, solar energy (SE) applications, and heating and refrigeration systems. CFD and numerical investigations are expected to be beneficial tools for optimizing energy consumption in the aforementioned applications. Figure 1 provides an overview of the recently reported fields integrated with PCMs.

Application of PCMs in building compartments

Buildings account for between 30 and 40% of global energy usage [34]. The cooling of internal spaces demands a high amount of electricity consumption, leading to further GHG emissions. The majority of heat losses occur through window shutters, construction walls, roofs, and ceilings. TSS consisting of PCMs not only act as insulating materials in building construction but also store daytime energy from solar incident and release it during nighttime when the temperature drops below the PCM's melting point. Building thermal analysis is subject to complex and dynamic environmental conditions.

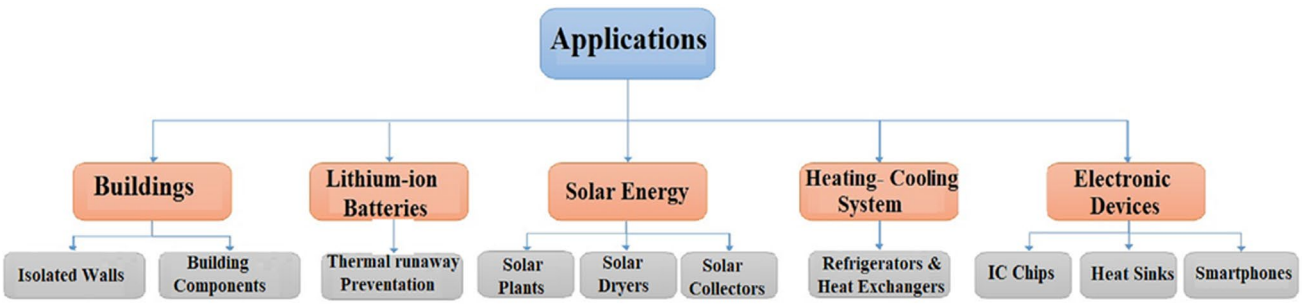

Fig. 1 The overview of utilizing PCMs as TESS in various engineering fields

Yu et al. [35] evaluated the thermal characteristics of a roof integrated with an outer-layer PCM. The shape-stabilized PCM was composed of PW and high-density polyethylene. PCM thicknesses and phase transition temperatures were the main focus of this study. The average temperature of the inner surface of the roof was found to be only minimally affected by the PCM layer thickness. When the PCM layer thickness exceeded 30 mm, its impact was no longer noticeable. The reduction factor of the roof decreased to roughly 0.03 for thicknesses greater than 30 mm and remained constant with a larger PCM layer. A thickness of 30 mm was recommended for optimal heat performance. Bhamare et al. [36] conducted a numerical study on a PCM-integrated roof using an inorganic salt hydrate with a melting temperature of 26 °C. The thermal performance of the PCM-integrated roof was compared with a roof without PCM at three different PCM slab inclination angles, considering the lag time and the decrement factor as the two major factors in determining the thermal performance of the energy storage system (ESS). Higher time lag and lower decrement were recommended for better efficiency, which were obtained at a PCM slab inclination angle of 2°. At this angle, heat gain savings of up to 16% were achieved. It was indicated that the use of PCM reduced temperature fluctuations of the ceiling during morning hours. They developed a 3D model and applied the enthalpy–porosity method, which was believed to yield better results for narrower temperature ranges [37]. For further accuracy, radiation and convection effects, such as wind velocity and external combined convective heat transfer coefficient (HTC), were defined in C++ and imported as a user-defined function (UDF) into Ansys Fluent. Dabiri et al. [6] analyzed the thermal behavior of a brick integrated with RT35 as a PCM and ten air cavities for insulation purposes and improved strength. The brick was placed between outdoor and indoor air conditions on a hot summer day and a cold winter day. A transient, pressure-based two-dimensional (2D) model was used for CFD investigation. The external air temperature was considered as a function of time to examine the influence of daily temperature fluctuations on the thermal characteristics of the brick with and without PCM and air cavities. Hourly temperature profiles were imposed as UDF in Fluent. The authors concluded that on cold days, PCM storage primarily contributes to sensible heat rather than latent heat due to the melting range of RT35. On hot summer days, the LHS of PCM plays a significant role. In summary, PCM-integrated bricks can maintain human comfort temperatures. Tokuc et al. [38] studied daily PCM activation and its potential application in building compartments. Laboratory-scale experiments were conducted to represent a flat roof integrated with PCM. The effective parameters were adjusted based on the ambient seasonal climate conditions of Istanbul city. A 2D model was developed using Gambit for numerical investigations and imported into Ansys Fluent. Heat transfer in the PCM element was considered one-dimensional, neglecting the natural convection effect within the PCM. The upper and lower surfaces, representing the roof and ceiling, were treated as time-dependent. Therefore, a UDF was developed based on the experimental analysis data. Simulations were performed with PCM thicknesses of 1, 2, 3, 4, and 5 cm, and the results showed better thermal performance with a 2 mm thickness. The latent heat effect of RT27, used as the PCM in their study, was noticeable during transitional months such as September and May. The authors concluded that under severe climate conditions, PCM may not function appropriately due to incomplete melting and solidification cycles, emphasizing the need for careful technical and environmental analysis before choosing PCM for building applications. Diarce et al. [39] tested different radiation and turbulence models to investigate the thermal and airflow characteristics of a ventilated facade integrated with PCM. The RNG k–ε, standard k–ω, and SST k–ω turbulence models were compared with numerical and experimental data to select a suitable model for further research. The surface-to-surface and discrete ordinates models were used separately to account for radiation effects. The 2D geometrical model included a macroencapsulated PCM (RT35) sheet, an air channel, insulation plates (Styrodur XPS), brickwork, and an inner wall plasterboard. To model the PCM, the enthalpy–porosity and variable Cp approaches were tested, and the results indicated that the convection effect inside the PCM could be neglected due to its paraffinic nature. Therefore, the variable C_p method was used for further investigation due to its lower computational effort. The authors concluded that the surface-to-surface radiation model was not suitable compared to the discrete ordinates model and emphasized that radiative heat exchange between inner surfaces should not be neglected. Among the turbulence models, the RNG k-model performed better in the turbulent flow regime, while the standard k– and SST models performed adequately in the transitional regime of airflow. Khattari et al. [40] investigated the thermal and energy advantages of employing PCM in a ventilated room with a controlled cooling ceiling system. The primary objective of this study was to evaluate the potential of using paraffin C13 PCM to improve the performance of a cooling ceiling system integrated into a well-ventilated room. The study reported savings in cooling power of 17.07% and 16.30%, respectively, which represented a reduction in indoor air temperature fluctuation. Wang et al. [41] numerically studied the effectiveness of applying a movable PCM design to prefabricated temporary houses in different climate regions globally to improve their indoor thermal environments in

July. The results demonstrated that the implementation of the movable PCM design led to lower indoor air temperatures in all 12 selected cities, with greater effectiveness observed in seven cities located in tropical regions.

The results obtained from CFD simulations have demonstrated the enhanced thermal storage capabilities of building compartments integrated with PCMs. However, it is imperative to carefully consider the melting and solidification points of the PCM in order to ensure compatibility with the prevailing climatic conditions. Another crucial factor in designing a cost-effective TSS for building applications is the thickness of the PCM layer. By employing accurate CFD simulations, the optimal PCM thickness can be determined, thereby facilitating the achievement of desired thermal performance.

Lithium-ion batteries and thermal runaway prevention

Lithium-ion batteries have gained significant interest as energy storage solutions for EVs due to their exceptional electrochemical performance, extended cycle life, and lightweight nature [42]. However, these systems are prone to thermal runaway, typically resulting from mechanical impacts like nail penetration. Insufficient heat dissipation leads to operational failures and an increased risk of explosions. Air and liquid cooling systems are commonly employed for thermal management of lithium-ion batteries [43, 44]. Nonetheless, the inclusion of additional pumps, pipes, and complex infrastructures introduces high costs and restricts on-board applications. Recent studies have explored the integration of PCMs in TMS for lithium-ion batteries, as they offer lower maintenance costs and simplified design procedures.

One study focused on numerically investigating a hybrid thermal management system for lithium-ion capacitors in high-power applications, utilizing a 3D model [45]. The researchers combined PCM with flat heat pipes in the lithium-ion capacitors and subjected them to a rapid charge/discharge current rate of 150 A to assess the thermal behavior of the capacitors. They observed that integrating heat pipes into the PCM enhanced the uniformity of temperature distribution. Moreover, the natural convection in heat pipes helped mitigate the thermal conductivity challenges associated with PCMs. Sun et al. [46] proposed novel PCM-fin structures comprising longitudinal fins and cylindrical rings for thermal management of lithium-ion batteries. The study investigated the effects of various parameters, including the number of longitudinal fins, the position and number of cylindrical rings, and the heat generation rate. To establish a dimensionless distance metric, the ratio of the ring's radial distance to its diameter, denoted as "d*" was introduced. Different distance ratios (0, 0.1, 0.2, and 0.3) were examined, and it was determined that $d^* = 0.2$ yielded the most favorable results. The impact of the number of longitudinal fins (N) was further explored for the optimum case of $d^* = 0.2$. It was observed that temperature decreases as the number of fins increases, particularly at higher heat generation rates. For this case, a configuration with eight longitudinal fins was recommended. However, it was noted that using more longitudinal fins could reduce the amount of PCM and result in decreased availability of latent heat. Figure 2 illustrates the liquid fractions and temperature distribution corresponding to different longitudinal fin numbers.

Qian et al. [47] conducted a numerical investigation to examine the thermal efficiency of lithium-ion batteries equipped with a liquid cooling system utilizing an aluminum cold plate, specifically for high-power ES devices. The laminar model was created using ICEM CFD, and numerical calculations were performed in FLUENT 14.0. A UDF was utilized to define the heat source. The results demonstrated a relative error of less than 2.7%. The study also revealed that the number and width of channels significantly affect the maximum temperatures of the battery pack, pressure drop, and cooling performance, emphasizing the existence of an optimum value for these parameters. In another study, Verma et al. [48] numerically investigated the impact of ambient air temperature on Li-ion battery packs. Non-paraffin capric acid was chosen as the PCM, with thicknesses ranging from 3 to 12 mm. The simulation considered two ambient temperatures, 298 K and a harsh desert temperature of 323 K, and examined the effects of high and standard heat generation rates of 63,970 W m^{-3} and 6870 W m^{-3} (2C and 3C, respectively). At lower discharge rates, the battery temperature increased by up to 2 K and 1.7 K under sub-ambient and hyper-ambient conditions, respectively, with satisfactory performance from capric acid. At higher discharge rates, such as during high-speed acceleration in EVs, the temperature rose to 312 K at 294 K ambient temperature, but capric acid reduced it to 305 K. Under hyper-ambient temperatures, a thickness of 12 mm was more effective in mitigating localized heat generation, lowering the temperature from 342 to 333 K. Capric acid demonstrated better temperature reduction with a thickness of 3 mm compared to hexadecane as a PCM with a thickness of 9 mm, highlighting its cost-effectiveness. The thermophysical properties of paraffin/expanded graphite PCM in a battery thermal management system were studied by Ling et al. [49] The synergistic effects of the mass fraction of paraffin in the composite and the density of packing were examined to determine the optimal composition. Most paraffin-based PCMs have low thermal conductivity, prompting the integration of expanded graphite to enhance thermal conductivity and facilitate faster HTR and improved temperature uniformity. The study recommended a PCM with a melting point of 44 °C for battery thermal management. Higher density of PCM resulted in a slower temperature rise rate, but excessively high density compromised the

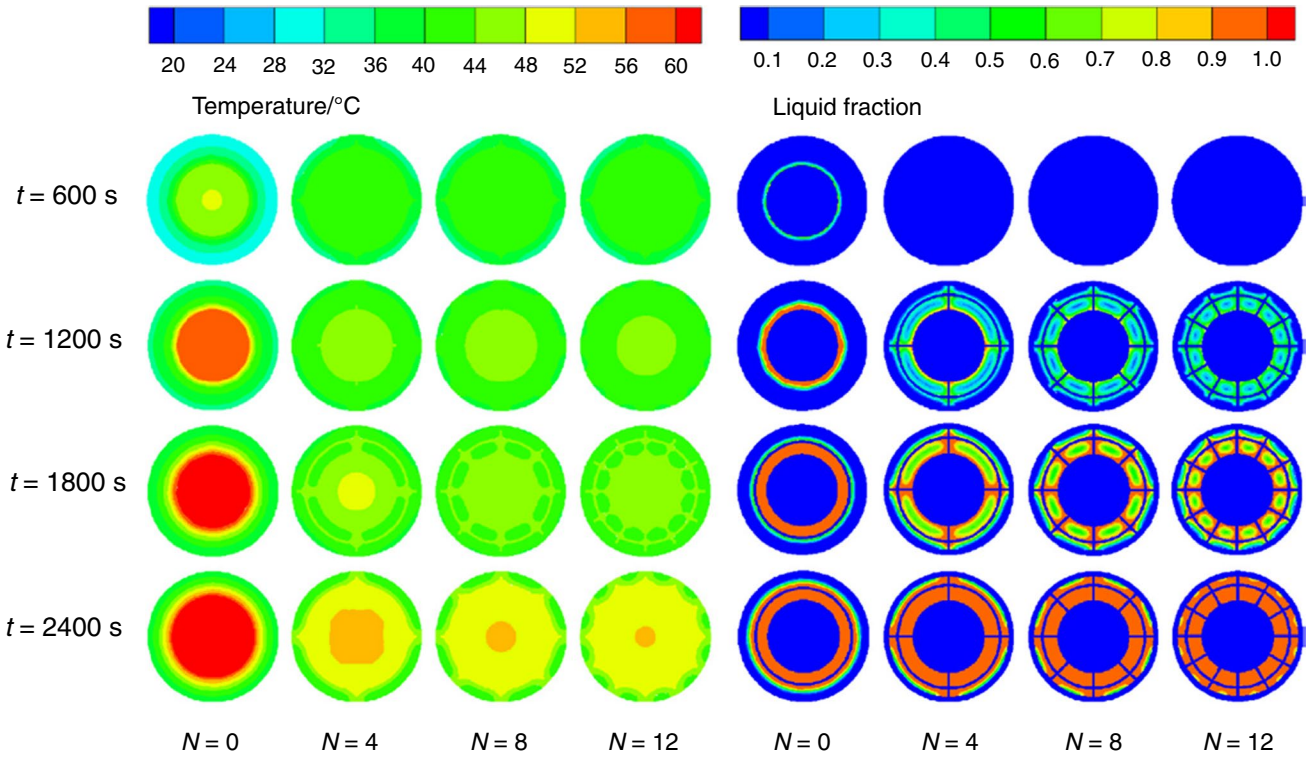

Fig. 2 Contours of temperature and liquid fraction within the BTMS for different numbers of longitudinal fins presented by Sun et al. [46]

porosity of the expanded graphite matrix, causing paraffin to squeeze out. Kshetrimayum et al. [50] proposed a hybrid PCM-liquid plate cooling system for thermal management of battery packs in EVs. Module A, consisting of 10 cylindrical cells arranged in 2 rows with 5 cells in each row (type 18,650 lithium-ion), was considered. The sides of the cells were equipped with microchannel plates, while one was placed in the center. It has been previously mentioned that mechanical events and accidents, such as nail penetration, have significant impacts on battery performance. Therefore, the temperature distribution and thermal behavior under normal discharge, nail penetration events, and thermal abuse conditions were analyzed. For the analysis, the Newman 2D pseudo electrochemical model, short-circuit model, and thermal abuse model were employed as UDFs to define heat generation rates using Ansys Fluent 18.1 [51, 52]. An et al. [53] conducted a CFD numerical investigation to assess the thermal performance of a composite phase change material (CPCM) consisting of paraffin (RT44HC) and expanded graphite EG integrated into a lithium-ion battery module with a liquid cooling system (water). Various operational and layout parameters were explored, including liquid flow velocity, battery channel order, mass fraction of EG as an additional component of the CPCM, and charge–discharge cycles. The heat generation rate of the lithium-ion battery was calculated for the different discharge rates based on the 3D model presented by Bernardi et al. [51], which is derived from the electrochemical reaction inside the cells. They observed no significant thermal characteristics variations when the EG mass fraction increased from 6 to 20%; however, a heat dissipation reduction was noted when the mass fraction reached above 30%, due to the higher thermal conductivity of CPCM, which resulted in lower latent heat. They concluded that the CPCM with 6% EG satisfies the required heat dissipation for all the charge and discharge duties for liquid velocities lower than 0.04 ms^{-1}. The schematic model and the generated mesh are displayed in Fig. 3. Xin et al. [54] conducted a numerical study on a hybrid cooling system that combines a CPCM and counterflow liquid cooling, aiming to enhance the thermal performance and safety of a lithium-ion battery operating at 40°C. The study investigated the effects of various parameters, including the thicknesses of the composite PCM, coolant flow directions, mass fractions of EG, and inlet velocities and temperatures of the coolant, on the maximum temperature and temperature uniformity of the battery module. The results indicated that the hybrid cooling system effectively manages rapid discharging and high-temperature environments. The optimal mass fraction of EG was determined to be 12%, and a CPCM thickness of 4mm was identified as the optimal condition.

The literature review reveals the potential of PCMs for TMS in lithium-ion batteries. CFD simulations have been

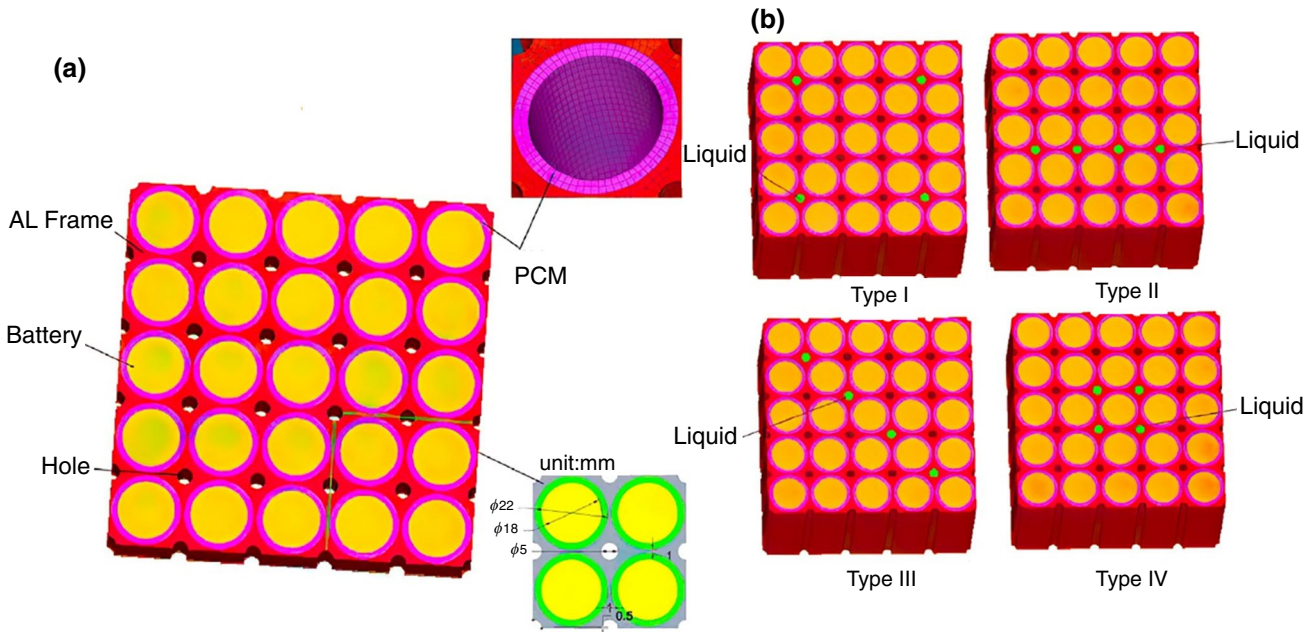

Fig. 3 Mesh model of the battery module. **a** The geometry dimensions and mesh model of the ITMS. **b** Four layouts of liquid cooling channels presented by An et al. [53]

extensively used to investigate heat transfer characteristics and mitigate thermal runaway issues caused by nail penetration under normal and high heat generation conditions. To ensure accurate and realistic simulations, the heat sources of lithium-ion batteries are defined based on charging and discharging reactions obtained from electrochemical models UDFs integrated into the simulation software. Considering the relatively low thermal conductivity of certain PCMs in lithium-ion battery applications, composite materials have been developed to enhance their thermal performance. The physical properties of these composite materials can be easily defined in the simulation software, enabling optimization of the material composition for lithium-ion battery applications. Another approach to overcome the thermal limitations of PCMs involves incorporating additional convection systems. CFD serves as a valuable tool for predicting and analyzing the synergistic effects of thermal management techniques, such as the combination of PCMs and liquid or air convection systems.

Solar energy utilization and storage systems

The utilization of SE as a clean, renewable, and environmentally friendly resource has gained significant attention in efforts to reduce reliance on fossil fuels. SE can be harnessed either through photovoltaic panels to generate electricity or directly as a heat source for various domestic and industrial applications [55]. While direct solar radiation is essential for the operation of photovoltaic panels, it is equally crucial to regulate their temperature rise in order to maintain optimal efficiency, as the electrical performance of photovoltaic panels tends to decrease with increase in temperature [56]. On the other hand, the limited availability of SE for heating applications poses a significant challenge, as access to SE varies throughout the day and night and is influenced by seasonal and geographic factors. To overcome this limitation and enable energy storage and release during peak-on and peak-off periods, PCMs have been widely recognized as the most effective materials.

Chaabane et al. [57] conducted a numerical investigation on an integrated collector storage solar water heater, utilizing myristic acid and RT-42 graphite as PCM. CFD models were developed to analyze the LHS performance of a cylindrical water tank mounted on a parabolic concentrating reflector, as illustrated in Fig. 4. The study revealed that myristic acid exhibited superior performance due to its higher melting point temperature. Additionally, the effect of PCM radius on the storage tank was examined, considering three different values ($R = 0.2$ m, $R = 0.25$ m, and $R = 0.3$ m). The results showed that the lower radius value achieved higher water temperatures, while larger radius value had a negligible impact on energy-saving efficiency, with a temperature difference of approximately 1°C.

Fornarelli et al. [24] conducted a study on the heat exchange characteristics of a single shell and tube LTES system for concentrated solar plants. The chosen PCM was a binary eutectic salt ($NaNO_3$-KNO_3 60–40 mass%). The investigation focused on analyzing the effects of conduction

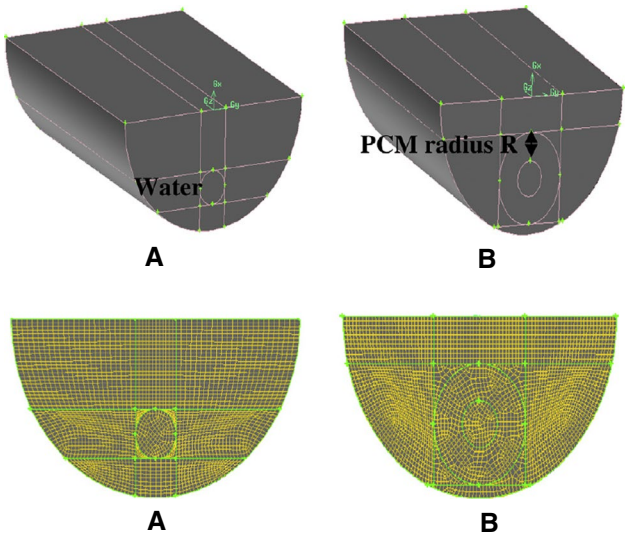

Fig. 4 Described model and the generated mesh for an ICS system without PCM and with a PCM of radius $R = 0.3$ m presented by Chaabane et al. [57]

and convection heat transfer within the PCM domain. Initially, conduction was found to be the dominant heat transfer mechanism in the radial direction for time intervals less than 1 h ($t < 1$ h). As the process progressed into the second stage (1 h $< t < 2$ h), the PCM began to melt, leading to the occurrence of natural convection and subsequent improvement in heat transfer. To isolate the pure conduction effect, the buoyancy term in the momentum equation was set to zero, thus inhibiting fluid motion within the liquid PCM. When natural convection was allowed, the stored heat reached approximately 90% of the maximum in around three hours, surpassing the heat transfer achieved through conduction alone. Further analysis of the mushy zone parameter (A_{mushy}) revealed its influence on surface heat flux, as well as the movement and convection of the liquid phase during the melting process. Higher values of A_{mushy} resulted in a slowdown of convection. In a separate study, Raj et al. [58] investigated the fundamental conduction–convection heat transfer mechanisms in a cylindrical macroencapsulated structure filled with PCM, which was applied to a solar air heating system. The charging and discharging processes were analyzed for cases involving conduction alone and a combination of conduction and convection. In the case of conduction alone, the bottom face was solely heated through conduction from the absorber surface, where solar radiation was provided. To account for the fluctuating solar heat flux, a UDF was added to the solver. The results indicated that a minimum solar radiation of 400 W m^{-2} (over 5000 s) was required to initiate the melting process, and conduction alone was insufficient to achieve complete PCM melting. When conventional heat transfer via air was employed, the solid PCM region in front of the flow direction melted more rapidly compared to the trailing side. However, due to flow detachment, the melting process was less effective at the rear side of the cylinder. The researchers suggested that encapsulated PCM with working fluid passage could induce turbulence and enhance heat transfer. Bashir et al. [59] proposed a novel dish-micro gas turbine system with a solar receiver integrated with PCM to mitigate thermal fluctuations, act as a thermal storage unit, and optimize design parameters through CFD simulations. The author highlighted the significant issue of convective and radiative heat losses in concentrated solar receivers, particularly at high temperatures, which can lead to thermal heat exchange failure and system damage. Therefore, maintaining stability in the outlet fluid temperature is crucial. However, the literature lacked knowledge about the properties of PCMs required for high-temperature performance, posing a challenge in material selection. A PCM with high thermal conductivity is necessary to achieve uniform temperature distribution. Among the analyzed materials (Mg_2Si, MgSi, and AlSb), Mg_2Si exhibited superior thermal conductivity and melting point, resulting in a more uniform temperature profile. The surface-to-surface model, combined with the ray-tracing model, was utilized to consider the constant solar heat flux [60]. It was found that a TS performance below 500 W m^{-2} would be insufficient to melt the PCM; thus, a minimum heat flux of 500 W m^{-2} was considered to provide adequate latent heat. Ramana et al. [61] conducted an experimental investigation comparing the LHS system with the sensible heat storage (SHS) system in a solar stratified storage tank, validated with CFD simulations. The storage tanks were filled with HS58 as the PCM. The LHS system was divided into three zones, including a porous zone, while the SHS system was treated as a single fluid zone. The results revealed a temperature stratification with higher temperatures at the top and lower temperatures at the bottom of the cylinder in the LHS system, which favored the desired stratified flow. Moreover, the presence of PCM balls in the mid-zone of the LHS system reduced mixing effects, maintaining an undisturbed cold bottom zone. The LHS case exhibited a maximum heat storage capacity of 256.7 MJ, compared to 225.0 MJ for the SHS tank. Additionally, the LHS system demonstrated a shorter charging time, resulting in significant energy savings. Iranmanesh et al. [62] proposed a numerical investigation of a solar cabinet dryer that incorporated a heat pipe evacuated tube solar collector and a storage tank integrated with an ESS in the form of PCM (Fig. 5). The integration of PCM in the solar cabinet dryer was intended to preserve the quality of the feedstock by indirectly exposing it to SE, making it suitable for nighttime operation. PCM selection was based on the higher thermal storage capacity of PW. In order to consider the effects of viscosity on convection during the phase change process, the dynamic viscosity of PCM was considered as a function of temperature.

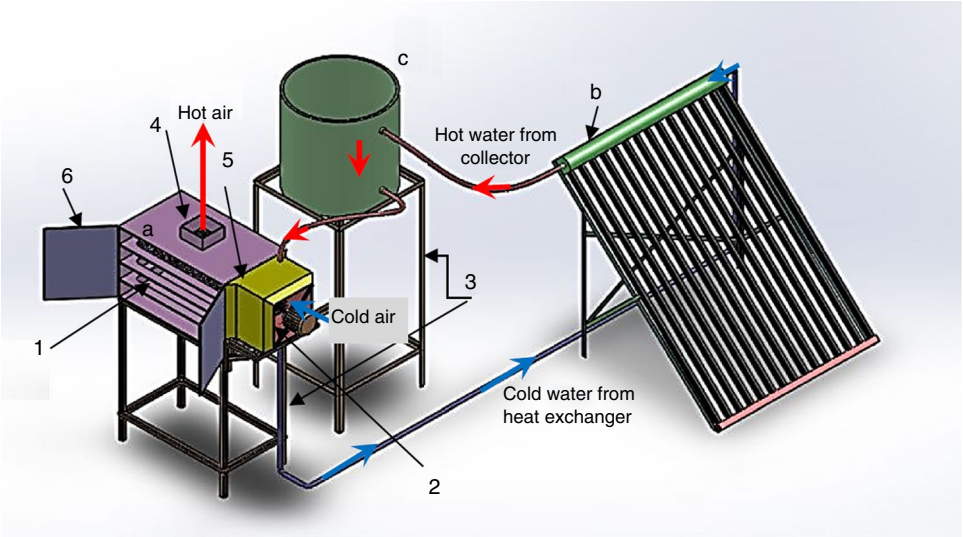

Fig. 5 The schematic of solar cabinet dryer including **a** Dryer; **b** Evacuated tube solar collector; **c** Storage tank and PCM container inside presented by [62]

CFD results for the discharging process with an airflow rate of 0.025 kg s^{-1} showed that thermal contours around the PCM were relatively higher, leading to higher inlet air temperatures for the drying process. The velocity streamlines revealed turbulent airflow at the bottom of the cabinet, which could have an impact on the trays located there. Figure 6 presents a comparison of the stored energy for cases with and without PCM. Al-Najjar et al. [63] employed a novel mathematical model for a photovoltaic/PCM system, which offers faster and more user-friendly calculations compared to existing CFD models. The proposed model was validated through both CFD simulations and experimental verification, demonstrating high accuracy with significantly reduced computation time. Additionally, a case study was conducted to investigate the system's characteristics and parametric performance, resulting in the development of design charts for two system indices: PCM melting time-interval and thermal efficiency. The findings emphasized the significance of the average PCM temperature in the mathematical modeling of the system, and they revealed a logarithmic proportionality between thermal efficiency and solar radiation.

Heating and cooling systems integrated by passive TES

Domestic and industrial refrigerators and freezers consume significant amounts of energy during their continuous daily operations. The increased working cycles of the compressor are primarily attributed to heat loss from the refrigerating containers. To enhance the efficiency of the refrigeration process, the integration of thermal LHS with PCMs has emerged as a novel technique. PCMs effectively absorb heat isothermally during the phase change process, resulting in

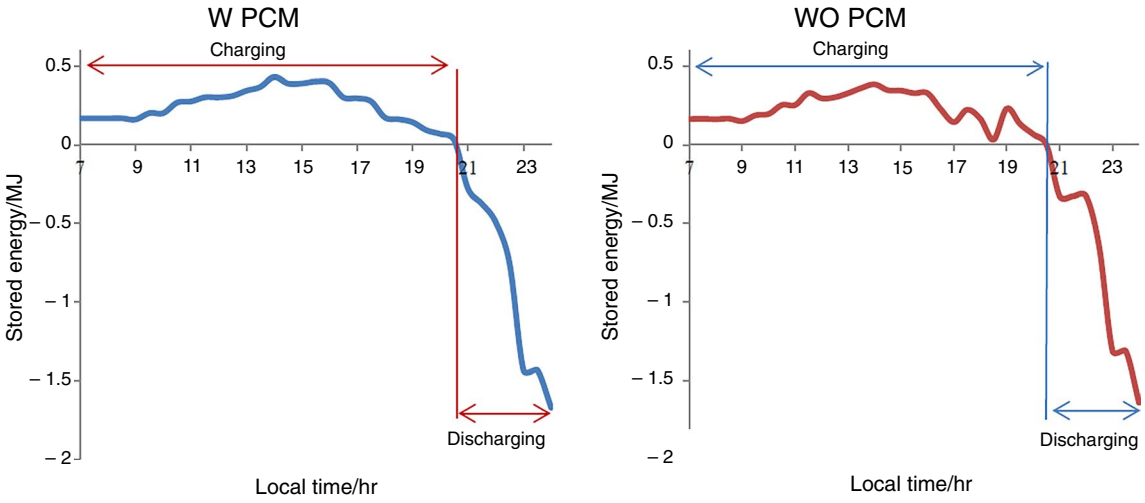

Fig. 6 Changes of the energy that has been saved in a storage tank both with and without PCM presented by Iranmanesh et al. [62]

a constant temperature within the container until complete melting occurs. This characteristic extends the off cycle of the compressor and significantly reduces electricity consumption, making it a desirable feature for energy efficiency improvements.

Pavithran et al. [64] conducted an investigation on a refrigerator incorporating PCM and explored different configurations of PCM-containing storage boxes. The incorporation of PCM showed promising results in maintaining the temperature inside the refrigerator during compressor off-time, leading to significant energy savings. The combined horizontal and vertical configuration of PCM incorporation was found to be the most effective in stabilizing the temperature within the system. Zarajabad et al. [65] conducted numerical investigations to analyze the impact of PCM volume on the cold TSS, employing various PCM thicknesses. The study considered seven PCM containers with different solidification and melting times, and the simulation results were successfully validated against experimental findings by Marques et al. [66]. The eutectic solution of NaCl–H_2O was selected as the PCM based on the ASHRAE standard, and cubic geometric configurations with dimensions of $h \times 28 \times 43.5$ cm^3 were utilized, where h represented the PCM thickness ranging from 0.5 to 6 cm. The useful working time of the cold TSS, denoted as τ_{disch}, expressed in hours per unit mass of PCM (kg), was used to evaluate the system's performance. The results indicated that increasing the PCM thickness resulted in an increase in occupied volume and τ_{disch}. Notably, a significant improvement of 45% in τ_{disch} was observed when increasing the PCM thickness from 2 to 3 cm. Subsequently, τ_{disch} remained relatively constant, suggesting that 3 cm was the optimum thickness for the cold TSS. Elarem et al. [67] studied the energy efficiency performance of a household refrigerator integrated with a eutectic NaCl-H_2O mixture as PCM. The results calculated a 12% reduction in power consumption and an 8% increase in coefficient of performance using PCM. In order to investigate the impact of PCM placement, a numerical analysis was performed to examine temperature distribution and airflow velocity within the refrigerator compartments. The authors concluded that "case-4," which involved occupying the evaporator with PCM, adding horizontal racks covered with PCM to the compartment, and vertically mounting a rectangular parallelepiped container filled with PCM in the refrigerator, exhibited the most uniform temperature distribution, shorter stabilization duration, and best energy performance. To optimize case-4, the influence of PCM coverage percentage (10%, 50%, 75%, and 90%) was examined. It was observed that lower time intervals were achieved with PCM coverage ranging from 10 to 50%, while no significant changes were reported for coverage percentages of 75–90%. Ezan et al. [68] proposed a 3D vertical beverage cooler with forced air circulation inside the container, integrated with a PCM slab. The influence of various slab thicknesses (2, 4, 6, 8, and 10 mm) on air velocity distribution and temperature variations was numerically investigated. A UDF was developed to analyze the compressor on–off controller and incorporated into the software. Due to the narrowness of the PCM slab, natural convection within the PCM was considered negligible, and the effective heat capacity method was employed to simulate the solidification–melting processes instead of the enthalpy–porosity method. A pressure jump was applied to simulate airflow across the fan, simplifying the simulation process. The results indicated that the incorporation of a PCM slab led to a reduction in maximum air velocity, and thicker PCM slabs required higher fan power. Specifically, the integration of a 2 mm PCM slab resulted in a significant reduction in the frequency of on–off cycles, approximately ten times fewer compared to the non-PCM condition. Additionally, a slab thickness of 6 mm was found to yield the minimum compressor run-time ratio, indicating the best cooling performance due to improved airflow circulation and uniform temperature distributions. Copertaro et al. [69] utilized the finite element method (FEM) in COMSOL Multiphysics to analyze the thermal characteristics of a refrigerated container envelope integrated with eight types of paraffin and one type of salt hydrate as PCMs. This analysis was performed considering the climate contexts of three Italian cities: Milan, Ancona, and Palermo. Five different heat source exposures were investigated as numerical case studies. The authors incorporated the temperature-dependent heat capacity of the PCMs into the software to obtain more realistic and accurate results. The numerical investigations revealed a deviation between the model predictions and the observed data. This deviation was attributed to the numerical model's underestimation of the daily maximum and minimum heat flux. Among the PCMs considered, paraffin RT35HC was identified as the most suitable choice for summertime in Milan, Ancona, and Palermo. This selection was based on its high thermal storage capacity and its melting temperature similarity to the ambient conditions. Hu et al. [70] investigated the integration of PCM storage with an HVAC (Heating, ventilation, and air conditioning) system to enhance energy flexibility. Both experimental and numerical methods were employed to achieve the optimal design of the PCM storage and assess its potential for energy savings. The experiments revealed that the quantity of PCM had a greater impact on the temperature of the PCM storage compared to the discharge inlet air temperature and airflow rate. Furthermore, the results indicated that PCM storage could reduce energy costs by 7% while maintaining comfortable indoor thermal conditions. However, the payback time for HVAC systems

with PCM was found to be seven years longer compared to HVAC systems without PCM. The study suggests conducting further research to explore the impact of PCM storage on night cooling and its potential for energy flexibility in different conditions and climates.

CFD analysis plays a crucial role in investigating refrigerators integrated with PCM, providing valuable insights into the optimal arrangement and placement of PCM within the container to enhance the hydrodynamic effects of airflow on the solidification and melting processes of PCMs. By utilizing CFD simulations, it becomes possible to obtain more accurate and realistic results regarding the behavior of PCM in refrigerators. To further improve the fidelity of the simulations, it is recommended to incorporate UDF that define the compressor's off-time and on-time, allowing for a more precise representation of the system dynamics. This approach enhances the accuracy of the simulations and enables a comprehensive analysis of the performance of PCM-integrated refrigerators.

Electronic devices and generated heat dissipation by PCMs

The advancement of electronic devices, characterized by their miniaturization and increased functionality, has posed challenges for engineers to address the issue of overheating, which can lead to operational failures. In response, researchers have been exploring innovative heat removal technologies to mitigate these problems. One emerging approach is the integration of PCMs and thermal conductivity enhancers within electronic devices, offering a passive thermal management solution for cooling purposes. By utilizing PCMs, which exhibit an isothermal process during phase transition and possess high energy density, more uniform temperature distribution can be achieved within electronic devices [71]. This approach showcases the potential of PCM-based cooling technologies in effectively addressing the heat dissipation requirements of modern electronic devices.

Kurhade et al. [72] conducted simulations using PCM cooling systems with PW as the PCM for electronic components simulated in smartphones. In their 3D model, the heat-generating elements were immersed in the PCM. The study concluded that the PCM significantly reduced the temperature and exhibited a delayed effect by absorbing latent heat from the electronic devices. Alshaer et al. [73] presented a numerical investigation to predict the thermal performance of an electronic device integrated with a porous carbon foam matrix filled with PCM and carbon nanotubes to enhance the low thermal conductivity of PCM. They applied carbon foam (CF-20) and PW RT65 as the PCM and simulated three different modules: pure foam, foam with PCM, and foam with PCM and carbon nanotubes, at carbon foam porosities of 55%, 65%, 75%, and 88%. The results showed an 11.5% temperature reduction on the module surface due to the higher thermal conductivity of carbon nanotubes with foam porosities below 75%. A temperature reduction of 7.8% was observed for 88% porosity, indicating that higher porosities lead to a lesser reduction in module surface temperature. Huang et al. [74] conducted a comprehensive study on the thermal characterization of wood's alloys (50Bi, 25Pb, 13Sn, and 12Cd)/EG composite as a TMS for electronic chips. Figures 7 and 8 demonstrate the experimental components and physical model, respectively. The study investigated the major influences of input power density, latent heat capacity, PCM's thermal conductivity, and thickness of the PCM layer using experimental and numerical approaches. It should be noted that the latent heat capacity and thermal conductivity of the PCM are intrinsic properties of the materials used, making them challenging to adjust experimentally. Therefore, only a numerical approach was employed to study these effects. The PCM substrate functioned as a conductive heat spreader for heat power densities below 20 kW m^2. For effective thermal management using this PCM, an input heat power of 30 kW m^2 or higher was recommended. Increasing the latent heat capacity resulted in a constant equilibrium temperature with longer cooling and critical time. However, when the substrate's thickness increased from 3.3 to 7.3 mm, a slight decrease in the equilibrium temperature was observed.

Tomizawa et al. [75] proposed microencapsulated paraffin with melamine resin and polyethylene composite sheets as

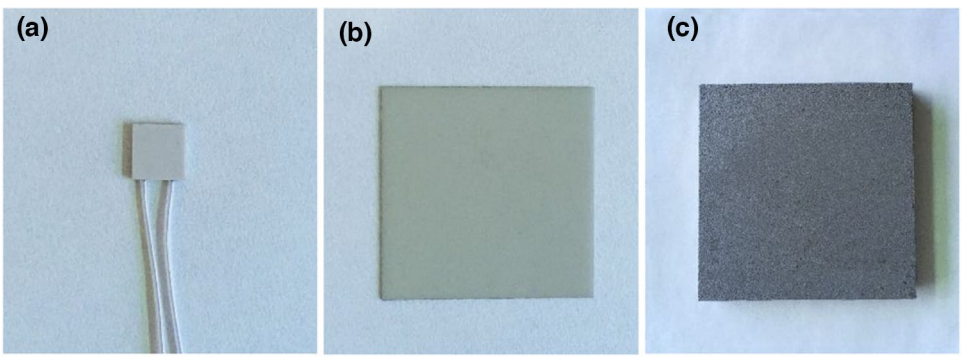

Fig. 7 Various components of the TMS: **a** chip, **b** AlN plate, and **c** PCM-based substrate presented by Huang et al. [74]

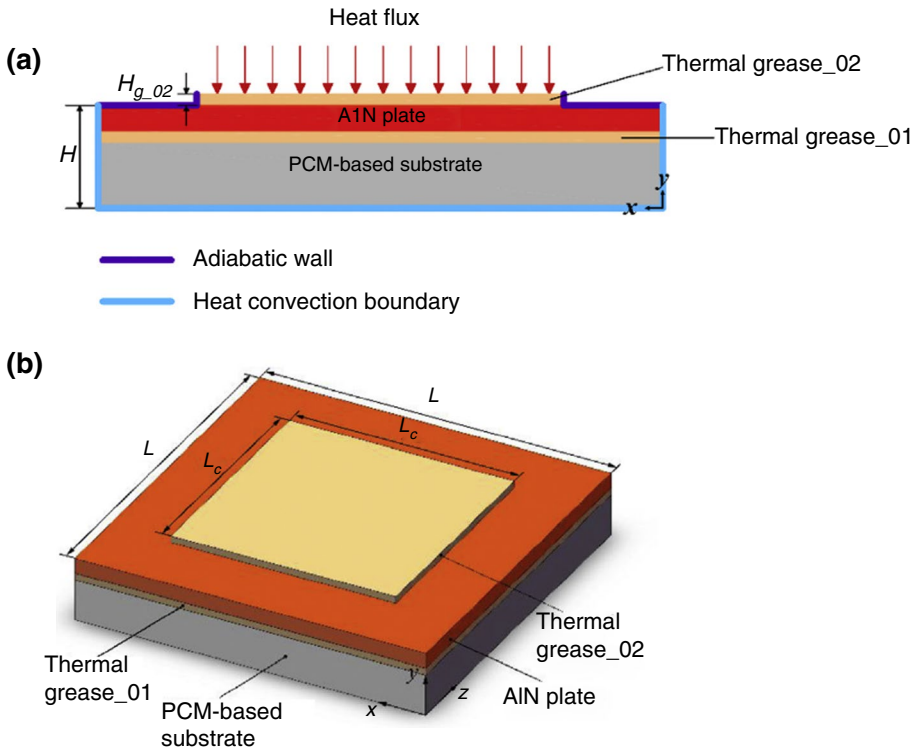

Fig. 8 Physical model of the TMS for numerical studies: **a** 2D, **b** 3D model presented by Huang et al. [74]

PCM to investigate the thermal management characteristics of smartphones. Both experimental and numerical studies indicated that the application of PCM sheets resulted in a delayed temperature rise, and a linear relationship was observed between the saturation time and the mass of the PCM sheet. Thicker PCM sheets demonstrated more effective thermal management. It is worth noting that the physical properties of the PCM were evaluated using the Bruggeman equation and the simple mixing rule. The results demonstrated good agreement between the experimental data and numerical simulations, suggesting that the mixing rule can be applied for estimating the physical properties of PCM composites. Arshad et al. [76] conducted a numerical study on heat sinks filled with n-eicosane as PCM, used for passive cooling systems of electronic devices, with fin thicknesses of 2 mm and 3 mm. Different heating power levels were considered to evaluate the optimal operating conditions and determine the best thermal storage system (TSS) configurations. The results indicated that a uniform, prolonged, and effective melting process was achieved with a fin thickness of 3 mm due to the lower number of fins compared to a fin thickness of 2 mm. The authors suggested that for higher heating power generated by electronic devices, a larger amount of PCM or a PCM with a higher latent heat is required to extend the melting time, which is crucial for maintaining lower base temperatures. Ghadikolae et al. [77] presented a numerical study on the laminar flow and heat transfer of a single-phase covalently functionalized graphene nanoplatelets (CGNPs)/H_2O green nanofluid in a liquid block heat sink. The heat sink incorporated novel fin designs and nature-based algorithms for central processing unit (CPU) cooling in electronic packages. The study investigated the impact of varying Reynolds number, nanoparticle volume fraction, and baseplate designs on the CPU temperature, pumping power, HTC, and thermal efficiency of the heat sink. The results demonstrated that the addition of nanoparticles to the base fluid reduced the maximum temperature of the liquid block. Increasing the nanofluid concentration and Reynolds number enhanced the overall thermal conductivity of the coolant liquid and improved the convective heat transfer, leading to a decrease in the CPU temperature.

Based on the review of the literature, it can be inferred that electronic devices operate at different power densities. CFD serves as a valuable tool for simulating the desired function of PCMs and selecting suitable materials. In specific cases where power densities are such that the PCM does not undergo melting, its role shifts to that of an insulating layer, potentially causing malfunctions in the TMS. Table 1 provides an overview of recent CFD studies conducted in the field, focusing on their application-specific aspects.

Geometric configurations of PCMs

The utilization of conventional PCMs is often hindered by their inherently low thermal conductivity, necessitating the incorporation of additive materials to enhance their thermal

Table 1 Summarized CFD investigations of LTES systems incorporated PCMs for application section

References	Application	PCM	Geometry	Dimension	Discretization method	Numerical solution method	Assumption	Validation
Diarce et al. [39]	Complex façade systems	Paraffin	Rectangular	2D	FVM	Enthalpy–porosity method	PCM is a solid material	Experimental
Copertaro et al. [69]	Refrigerated containers in yards, ships & …	Paraffin/RT35HC	Rectangular cube	3D	FEM	Effective heat capacity method	Constant thermophysical properties of PCM except heat capacity Isotropic conductivity No mass transfers No convective heat transfer in the liquid PCM phase	Experimental
Dabiri et al. [6]	TSS (buildings)	Paraffin/RT35	Rectangular	2D	FVM	Enthalpy method/ enthalpy–porosity method	Laminar flow Constant density of PCM in all phases Boussinesq approximation (air density) Negligible convective heat transfer in solid zones	Alqallaf et al. [78]
Essid et al. [79]	Energy efficient buildings	Paraffin wax/polymethylmethacrylate	Cube	3D	FEM	Enthalpy method	Not mentioned	Experimental
Wang et al. [80]	Adaptive building roof	Polystyrene foam	Rectangular	1D	–	Enthalpy–porosity method	No absorptance on the transparent interface Equal reflectivity on both sides of the interface	Experimental
Alshaer et al. [73]	Electronic equipment	Paraffin/RT65	Rectangular	2D	FVM	–	Negligible convection heat transfer	–
Zhao et al. [81]	Electronic equipment	Paraffin/RT60	Cylindrical/rectangular (cubic)	2D	FVM	Enthalpy–porosity method	Laminar, transient, and incompressible flow Constant thermal properties of PCM in all phases Negligible viscous dissipation Boussinesq approximation	Experimental

Table 1 (continued)

References	Application	PCM	Geometry	Dimension	Discretization method	Numerical solution method	Assumption	Validation
Huang et al. [74]	Electronic equipment	Wood's alloy/expanded graphite composite	Square or rectangular cubic	3D	FVM	The equivalent specific heat capacity method	Homogenous and isotropic materials Ignored supper-heating and supercooling effects of the PCM During the heating and cooling process, all material volume variations were ignored	Experimental
Youssef et al. [82]	Heat exchanger/solar heating system	Paraffin/A16	Cylindrical/spiral	3D	FVM	Enthalpy–porosity method	Steady and incompressible flow Negligible viscous dissipation Constant properties Neglected natural convention effect for the PCM	Experimental
Zarajabad et al. [65]	Cold TES	NaCl-water eutectic solution	Rectangular cube	2D/3D	FVM	Enthalpy method	Constant thermophysical properties for the PCM Neglected convection heat transfer in melted regions Constant latent heat during a fixed phase change temperature Ignored supercooling effects	Marques et al. [66]

Table 1 (continued)

References	Application	PCM	Geometry	Dimension	Discretization method	Numerical solution method	Assumption	Validation
Ezan et al. [68]	Cold TES	Water	Rectangular cube	3D	FVM	Effective heat capacity method	Turbulent flow Air is Newtonian and assumed to be an incompressible fluid Constant thermo-physical characteristics for the PCM Negligible viscous heating, the radiative heat transfer, and natural convection inside the cooler	Experimental
Elarem et al. [67]	Cold TES	A4 PluseICE	Rectangular	2D	FVM	–	Constant physical properties of air except the density Boussinesq approximation Transparent air with negligible absorption and diffusion of radiation No melting/freezing process for PCM	Experimental
Bonamente et al. [83]	Heat exchanger/heat pump	Rubitherm™ paraffins	Cylindrical/cubic or square cube	3D	FVM	–	Not mentioned	Experimental
Peng et al. [84]	Heat pipe/lithium-ion battery	Expanded graphite	Cylindrical	3D	FVM	Enthalpy change method	Exposed heat pipe to ambient Adiabatic boundaries Appropriate equivalent heat transfer coefficient of boundary surfaces in contact with atmosphere Equality of initial cell and ambient temperatures	Experimental

Table 1 (continued)

References	Application	PCM	Geometry	Dimension	Discretization method	Numerical solution method	Assumption	Validation
An et al. [53]	Lithium-ion battery	Paraffin (RT44HC)/ expanded graphite composite	Cylindrical	3D	FVM	Enthalpy change method	Homogeneous physical properties of battery materials Constant and uniform internal heat of the battery Uniform current density throughout the battery during charge–discharge cycles	Theoretical
Javani et al. [85]	Lithium-ion battery/ electronic equipment	*n*-Octadecane	Rectangular cube	3D	FVM	Enthalpy–porosity method	Negligible melted PCM circulation Steady-state modeling Using average specific heat for the cell Free convection is the dominant heat transfer method	–
Kshetrimayum et al. [50]	Lithium-ion battery/ electronic equipment	Paraffin (2122carbon)	Cylindrical/rectangular cube	2D	FVM	–	Nail penetration is located at the center along the axial length of the battery cell Uniform and constant water inlet flow The rate in the cooling plate and the outlet flow to the ambient pressure	Kizilel et al. et al. [86]

Table 1 (continued)

References	Application	PCM	Geometry	Dimension	Discretization method	Numerical solution method	Assumption	Validation
Ling et al. [49]	Power batteries	Paraffin/expand graphite composite	Cylindrical	3D	FEM	Enthalpy method	Negligible density change due to solid-phase change Constant specific heat and thermal conductivity of the heaters and PCM Adiabatic boundary outside the composite PCM Infinitive PCM composite density	Experimental
Sun et al. [46]	Battery thermal management system	Paraffin	Cylindrical	2D	FVM	Enthalpy–porosity method	Boussinesq approximation for the linear density-temperature Relation	Experimental Wang et al. [87]
Verma et al. [48]	Lithium-ion battery/electronic equipment	Capric acid	Rectangular	3D	FVM	Enthalpy method	No flow case for melted PCM Keeping the initial temperature, the same as the ambient temperature Uniform heat generation in battery	Javani et al. [88]
Bashir et al. [59]	Dish-Micro Gas Turbine/solar system/solar heater	Mg_2Si/MgSi/AlSb	Cylindrical	3D	FVM	Enthalpy–porosity method	Adiabatic receiver outer wall Negligible buoyance effects in the PCM domain	–
Chaabane et al. [57]	Solar water heater	Paraffin RT42-graphite/myristic acid	Cylindrical	3D	Not mentioned	Enthalpy–porosity method	Incompressible fluid Fairweather condition Constant thermophysical properties of PCM except heat capacity Boussinesq approximation	Chaouachi et al. [89]

Table 1 (continued)

References	Application	PCM	Geometry	Dimension	Discretization method	Numerical solution method	Assumption	Validation
Fornarelli et al. [24]	Concentrated solar plants	Nitrate binary eutectic salt ($NaNO_3$-KNO_3, 60–40 mass%)	Cylindrical	2D	FVM	Enthalpy–porosity method	Axis, for the centerline of the axisymmetric geometry Adiabatic walls for the remaining external surfaces of the tube and of the PCM	Trp et al. [90]
Iranmanesh et al. [62]	Solar cabinet dryer	Paraffin/RT50	Cylindrical	3D	FVM	Enthalpy–porosity method	Constant thermophysical properties of the air Stationary at a uniform temperature of the computational domain as initial conditions Perpendicular solar radiation on the absorber plate of the collector	Experimental
Raj et al. [58]	Solar TSS (microencapsulated LHS system)	PW	Cylindrical/rectangular cube	3D	FVM	Enthalpy–porosity method	The interface formation during the phase transition has not been Tracked Constant thermophysical properties for the working fluid (ideal fluid) Isotropic solid and liquid PCM Neglected subcooling effects of PCM Ignored radiation models	Muhammad et al. [91]

Table 1 (continued)

References	Application	PCM	Geometry	Dimension	Discretization method	Numerical solution method	Assumption	Validation
Ramana et al. [61]	Solar TSS (SHS system)	HS58	Spherical/cylindrical	2D	FVM	Apparent heat capacity method	Insulated storage tank Laminar flow for the HTF Constant thermophysical properties of HTF except density Isotropic porosity and properties in the porous region	Experimental
Karami et al. [92]	Solar collector	Water/ethylene glycol	Cylindrical	3D	FVM	–	Same thermophysical properties of nanofluid and base fluid Suspension of nanoparticles in the fluid Ignored gravity effect	Chen et al. [https://doi.org/10.1016/j.expthermflusci.2008.05.008]

properties. However, this approach is limited in its advantages for large-scale PCM containers, such as building compartments, due to factors such as high cost, inadequate dispersion of nanomaterials, and poor stability. Consequently, researchers have focused on the optimization of geometric configurations to achieve desired charging and discharging rates for specific applications. Cylindrical geometries, such as shell and tube heat exchangers, are commonly employed for heating applications, while rectangular shapes are more suitable for electric devices and refrigeration purposes [93]. Spherical configurations are frequently used for encapsulated PCMs and concentrated solar receivers. Moreover, the inclusion of internal fins and extended surfaces has been extensively investigated to improve heat transfer within PCM enclosures. These studies primarily concentrate on the dimensions of the fins, including length, number, thickness, angle, and spacing within the enclosures [94]. By employing comprehensive CFD analyses to examine various geometries and fin arrangements, and their influence on heat transfer characteristics, particularly natural convection, researchers can determine the optimal configuration for enhanced performance.

Cylindrical-shaped case studies

Hosseini et al. [95] conducted a comprehensive investigation, combining numerical simulations and experimental analysis, to examine the thermal behavior of a LTES system during the charging and discharging processes of paraffin RT50 as the PCM. RT50 in a shell and tube LTES unit. The study demonstrated a direct correlation between the inlet temperature of the HTF, specifically water, and HTR. Increasing the inlet HTF temperature resulted in reduced PCM melting times and increased energy charging or discharging capacity, thereby improving energy efficiency. The heat transfer mechanism within the PCM involved a combination of conduction and convection, with conduction dominating during the initial stages of the charging process, followed by the prevalence of convection during the phase change processes. Kozak et al. [96] investigated the phenomenon of close-contact melting in a vertical double-pipe concentric storage unit with a circumferentially finned inner tube and a non-isothermal base. The study employed theoretical, numerical, and experimental approaches to analyze the process. The presence of fins in the inner tube played a significant role in accelerating the heat transfer process, resulting in a faster HTR and shortened charging time. The analytical model developed in this study revealed the dimensionless governing parameters of the problem, highlighting the dependence of the melt fraction on the FoSte3/4 (Fourier and Stephan) group. The fins not only facilitated enhanced heat transfer but also influenced the radius and time evolution of the thin molten layer between the fin and

PCM. The study suggested that applying heat to the outer shell of the LTES unit to initiate melting and establish close contact could effectively increase the HTR, ultimately leading to improved performance. Liu et al. [97] conducted a numerical study on the melting process of paraffin RT27 in a cylindrical TS apparatus that contained arranged arrays of heat sinks. It is noteworthy that the total area of the device, heat sinks, and filled PCM remained constant throughout the investigation. The study emphasized the crucial role played by the arrangement of heat sinks and the swirls induced by natural convection in the melting process. Considering these factors, it was observed that the local melting rate was faster when the interface was in contact with swirls, leading to the formation of cavities. Tay et al. [98] focused on the development of an appropriate correlation for fins applicable to the effectiveness-number of transfer units (e-NTU) approach for the first time. A vertical cylindrical heat exchanger, filled with PCM and equipped with a copper finned tube, was employed in this study. Water, RT32, and salt hydrate were used as PCMs. The study demonstrated that heat transfer by convection was negligible, and the number of fins required to achieve the desired effectiveness was determined. A similar approach can be extended to derive suitable equations for other fin arrangements, while accounting for natural convection through the development of appropriate correlations for effective thermal conductivity.

Jannesari et al. [99] conducted a comprehensive investigation on the heat transfer performance of cylindrical coils covered with thin diagonal rings and annular fins using both numerical and experimental approaches. Copper, known for its high thermal conductivity, was chosen as the material for the attached rings and fins. Additionally, a mixture of 30% ethylene glycol and 70% water was selected as the HTF. The presence of fins, particularly diagonal rings, significantly accelerated ice formation and enhanced its expansion. The thickness of the rings and the spacing between annular fins were optimized based on simulation results to maximize the total mass of ice formed. The researchers indicated that the optimal thickness of the rings depends on the thickness of the ice formed on the ring surface and the direction of heat transfer. In a study by Lohrasbi et al. [100], systems containing nano-enhanced phase change materials (NEPCM) were statistically evaluated with a focus on the discharging process in the presence of innovatively shaped finned heat pipes. The researchers simultaneously optimized a novel-shaped fin using a multi-objective response surface approach and CFD simulations to achieve the best design. The optimization process considered the relationship between the effective solidification capacity and the discharging rate as two vital parameters. The results demonstrated that the direction of change of fin branches does not significantly affect the discharging process. Moreover,

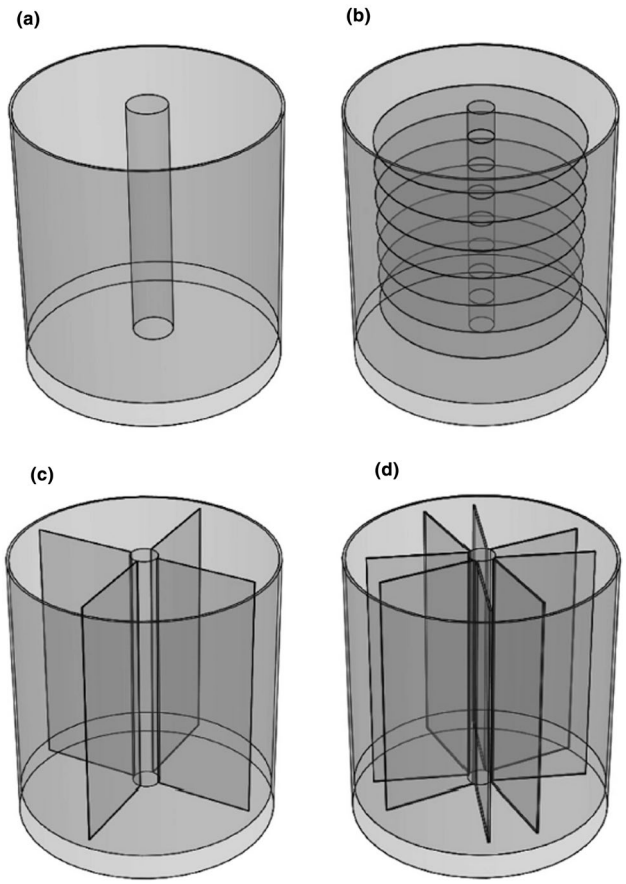

Fig. 9 Heat pipe-assisted LTESS in three dimensions, shown in **a** without a fin, **b** with a radial fin, **c** with a simple longitudinal fin, and **d** with an optimized V-shaped fin, presented by Lohrasbi et al. [100]

an increase in fin branch thickness leads to a reduction in the maximum effective solidification capacity. Notably, the enhancement in discharging rate resulting from an increase in fin branch length was found to be significantly greater than the effect of branch thickness increase on effective solidification capacity decrement. Consequently, the length of fin branches was maximized within the studied range, but not precisely equal to it, to maximize the discharging process. The addition of copper nanoparticles to water as the PCM was found to further enhance the discharging process. The geometric models and solid fraction contours for the optimized V-shaped fin case are illustrated in Figs. 9 and 10, respectively.

Bouhal et al. [101] conducted a numerical investigation on the melting process of pure gallium, serving as a PCM, in a cylindrical cavity with and without fins. The heat sources were designed with optimized geometries that considered the operating conditions and applied temperatures. The inclusion of four fins in the cylindrical cavity resulted in a higher heat flux within the PCM, leading to a reduced melting time (from 18.35 to 13.35 min when subjected to

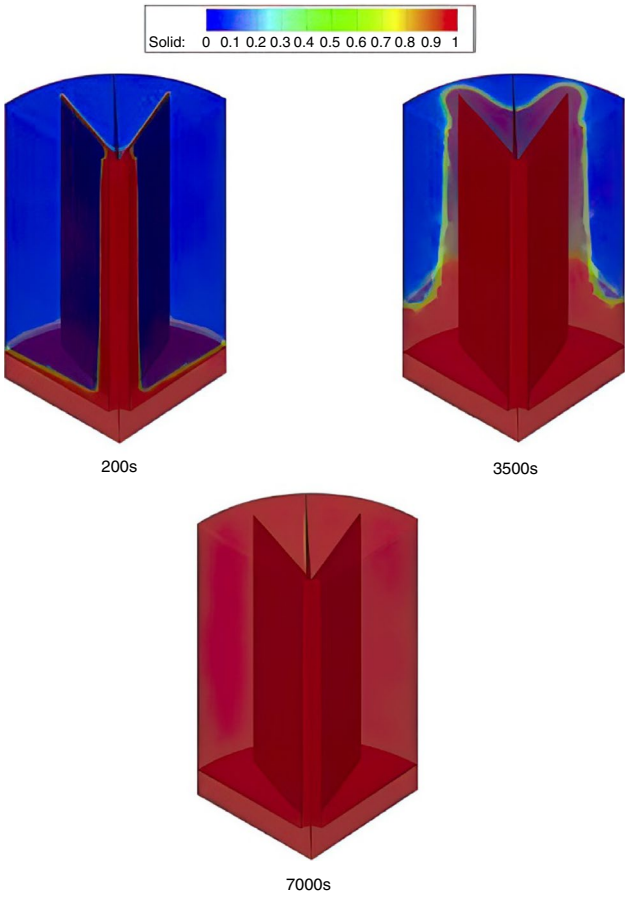

Fig. 10 Heat pipe-assisted LTESS solid fraction contour plot with an optimized V-shaped fin presented by Lohrasbi et al. [100]

a high temperature). Furthermore, the presence of inner heated source structures, whether equipped with fins or not, influenced the kinetics of gallium's melting. This effect was observed through isotherms, molten phase fraction, streamlines, and HTC distributions. The temperature of the melted zone in contact with the heating source progressively decreased, resulting in improved HTC values and enhanced charging and discharging rates of gallium. Figure 11 illustrates the liquid fraction contours for the case with fins, while Fig. 12 represents the same for the case without fins.

Soodmand et al. [102] conducted a numerical study to investigate the effects of different enclosures on the solidification and melting time of polyethylene glycol 1500. The results demonstrated that, at a given time, the cylindrical enclosure exhibited a higher amount of solidification liquid fraction compared to other geometries. The fastest melting time was observed in the horizontal rectangular and triangular configurations, which can be attributed to their sharp angles and the presence of long, flat bottom walls. These features are believed to have the most significant influence on natural convection. Zhu et al. [103] conducted a CFD simulation study to investigate the utilization of high-temperature PCM and supercritical CO_2 (S-CO_2) for latent heat storage in a cylindrical configuration. The study extensively discussed the impact of natural convection on the melting process of high-temperature PCM during charging and the heat transfer associated with energy release during discharging. The results highlighted the significant influence of natural convection on the melting process, emphasizing that the duration of natural convection plays a crucial role, and the time factor is more important than the maximum velocity in natural convection. Furthermore, the authors suggested that the performance of the system could be enhanced by utilizing cascaded high-temperature PCM, which could be a promising avenue for future research.

Rectangular-shaped case studies

The rectangular panel geometry with PCM was investigated by Prieto et al. [104]. They simulated the phase-changing processes of RT60 and palmitic acid. The study revealed that the vertical arrangement exhibited higher flow intensity values compared to the horizontal configuration for medium liquid fraction values of the PCM. Conversely, the horizontal configurations resulted in significantly higher flow intensity values for higher liquid fraction amounts of the utilized PCM, thereby highlighting the increased significance of natural convection. The results demonstrated that palmitic acid exhibited slightly higher heat transfer rates HTR for the vertical charging trend but took more time to complete the process due to its higher phase change latent heat. Significant differences were observed between the two types of PCM in the horizontally arranged plate during the melting process, particularly at the surface. However, similar curves and heat fluxes were observed during discharging for both PCMs, with negligible differences. These phenomena were attributed to the absence of convection heat transfer. The parametric study indicated that the optimized design and operating parameters have a substantial impact on the performance of the heat exchanger, with the melting process yielding higher values, except for the solidification of palmitic acid at lower thicknesses. Zhou et al. [105] performed a CFD simulation on the charging and discharging processes of salt hydrate as PCM filled in a rectangular-shaped container with rounded angles. In this model, the melting process was simulated using UDF codes for the source terms and solved using a pressure-based implicit algorithm. The results showed that after complete solidification, the latent heat was efficiently released, leading to a sharp temperature descent. It was also demonstrated that using multiphase models instead of solidification and melting models would facilitate unsteady simulations of supercooled PCM for long-term solar thermal storage. The

analysis of the discharging specifications of supercooled PCM revealed three distinct stages: stable supercooling, triggering crystallization, and regular solidification. The results indicated a rapid temperature rise of the PCM during the triggering crystallization period, followed by a small heat loss. Therefore, it can be concluded that the rectangular geometry enhances the heat flux between PCM and HTF due to its larger surface area, resulting in higher heat transfer rates. Ji et al. [106] investigated the effects of various fin length arrangement schemes (double fins attached to an aluminum-based rectangular container) on TESS. Commercial paraffin (RT42) was used as the PCM in this study. The Boussinesq approximation was employed to evaluate the impact of natural convection on the phase change medium due to its validity in considering density variations and buoyancy forces. The results obtained indicated that a fin length ratio (L_{upper}/L_{lower}) below 1, particularly $L_{upper}/L_{lower} = 0.25$, was more advantageous for enhancing PCM melting. This was attributed to the slowest decline rate of the Nusselt number, which significantly enhanced convection and improved the solid–liquid interface. It was concluded that the total thermal energy captured in the form of latent heat is nearly twice the value stored in the sensible type.

Zhao et al. [107] investigated the melting characteristics of a PCM inside a rectangular box with vertical straight fins to enhance heat transfer. The numerical study examined the impact of fin spacing and length for two different fin materials, namely aluminum and stainless steel. The results indicated that the optimal fin spacing is determined by the fin length, Rayleigh number, and Prandtl number, while the optimal fin length varies based on the thermal conductivity ratio between the fin and the PCM, fin spacing, and thickness, assuming negligible natural convection. The study derived theoretical correlations for the optimal fin spacing and length, which were then compared with numerical and experimental data. Further research in this area could contribute to the development of a comprehensive model capable of predicting the melting behavior of such latent heat thermal energy storage systems.

Spherical-shaped case studies

Arévalo et al. [108] investigated pool film boiling in a spherical geometry at saturated conditions, and in the absence and presence of radiation. The study demonstrated that the modeled system, when considering radiation in addition to convection, contrasted with existing correlations. Moreover, the researchers found that the heat flux exhibited periodic behavior as the vapor film thickness continuously changed. Amin et al. [109] investigated thermal interactions in a model of encapsulated spherical PCM (water and inorganic hydrated salt) that was filled with HTF. According to the results presented by Tay et al. [110], convection can be ignored and the PCM spheres' internal heat transmission can be precisely modeled using CFX. Furthermore, instead of employing a fixed number, the effective thermal conductivity was empirically determined, and this correlation can be used with the e-NTU approach to more accurately describe the melting process. The empirical equation performs well for hydrated salt mixtures with a single-point phase change and a density close to that of water. Enhancement of heat transfer in a TESS comprising an encapsulated PCM in a spherical geometry was investigated both numerically and experimentally by Aziz et al. [111]. Potable water and viscous Dynalene HC 40 were used as the PCM and HTF, respectively. In order to improve the system performance, pins and copper plating (copper coating to connect all the pins) were employed through CFD and experimental studies. The results obtained from the CFD and experimental analysis demonstrated that the use of pins and copper-coated capsules enhances HTR and significantly reduces the phase change time, which led to choosing this configuration as the optimal design option among the others. Cofré–Toledo et al. [112] investigated the encapsulation of spherical-shaped PCMs for latent heat thermal energy storage systems. CFD simulations were used to explore the melting and solidification processes of two commercial organic PCMs, RT5HC and RT10HC, in order to determine the behavior of the heat transfer coefficient (h) as a function of the liquid fraction and solid fraction of the PCM. Correlations for the Nusselt number as a function of the liquid or solid fraction were calculated, unifying the behavior of the fusion and solidification processes. These correlations are helpful in the design of TESS tanks for their application in heat-pump-type air-conditioning systems in buildings.

Arbitrary shapes

Tabassum et al. [113] performed a numerical study on the melting process of impure organic PCM inside an annular gap. The annular gap was created by an inverse outer equilateral triangular-shaped enclosure and different shaped inner tubes (namely circular, elliptical, and prolate), as shown in the schematic model in Fig. 13. They used a boundary-fitted coordinate technique and an enthalpy–porosity technique to simulate the system. It was found that the mushy zone increased at the top and bottom of the annulus and became thicker at the lower part during the charging process. The heat transfer rate (HTR) through conduction in the mushy zone was insignificant due to the lower thermal conductivity of the liquid PCM compared to the solid phase. The analysis showed that the maximum amount of stored energy differed

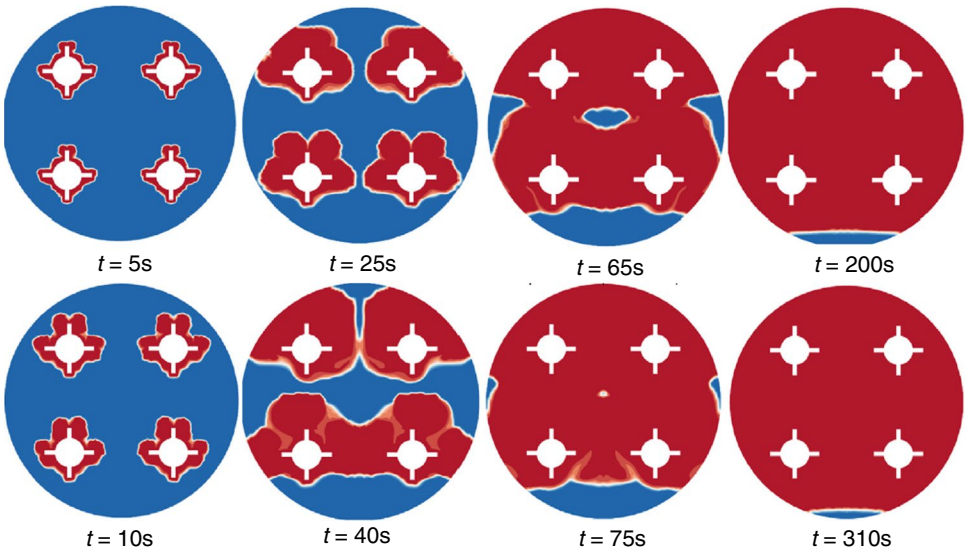

Fig. 11 Evolution of the liquid fraction of heating sources with fins (Th = 40 °C) presented by Bouhal et al. [101]

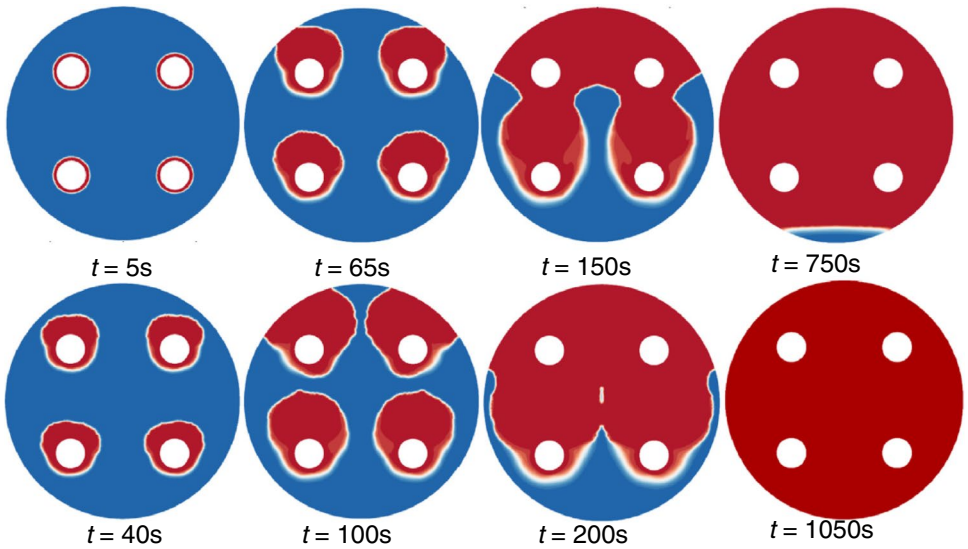

Fig. 12 Evolution of the liquid fraction of cylindrical heating sources without fins (Th = 40 °C) presented by Bouhal et al. [101]

among the different configurations at the same elapsed time. The investigation of inner tube shapes illustrated that the prolate-shaped inner tube exhibited a developed charging rate compared to the other two shapes. On the other hand, the oblate-shaped inner tube provided a higher stored energy capacity compared to the prolate-shaped tube. The researchers demonstrated that locating the inner tube in an eccentric position inside the inverse triangular annulus could result in a superior LTES device among the studied heat exchangers.

Elsayed et al. [114] studied the heat performance of an equilateral triangular-shaped enclosure filled with PCM, focusing on the improvement of LTES systems for solar heaters. It was mentioned that the practical application of this work is typically utilized in air-PCM heat exchangers [115]. Therefore, three triangular cylinders with the same volumes but different apex angles were investigated in the study. It was shown that the obtuse triangular cylinder exhibited higher temperature values at the rear vertical side, while the acute cylinder approached higher temperature values at the front portion and had the highest heat storage capacity. These findings indicate that the apex angle and the rear side of the triangle or container shape play an important role in the distribution of wall temperature, which significantly affects the heat storage capacity. Kasibhatla et al. [116] developed a numerical model to accurately simulate the thermal interaction between the heat transfer fluid HTF and PCM capsules in a storage unit. The numerical model consisted of distinct computational domains, including the HTF domain, capsule wall domain, and PCM domain, to reflect the physics in each domain continuum. In the HTF domain, equations describing forced convection and heat transfer were implemented, while a simple conductive energy equation with heat transfer was solved for the capsule wall domain. In the PCM

domain, a nonlinear enthalpy and temperature connection were used to compute a detailed solid–liquid phase change with solid settling. An efficient iterative technique for solid–liquid phase change was employed to describe this phase change in the PCM domain. The variable viscosity approach with implicit iterations compensated for solid settling in the PCM domain [117]. Photographic measurements were used to document the melt front of PCM during tests throughout the entire melting duration. The results indicated external heat transfer as well as PCM melting inside the capsule wall, which closely resembled trials conducted in a small-scale LTES unit with cylindrical capsules. Furthermore, the model demonstrated excellent agreement with an analytical estimation of thermal energy within a 2% error. Due to its refinement, the model can only be expanded to simulate the charging of a thermal storage unit with a small number of capsules. However, with sufficient computing resources and time, it could be employed for a complete storage unit with any number of capsules. Selimefendigil et al. [118] investigated the phase change dynamics of a 3D cylinder containing hybrid nanofluid and PCM. The PCM consisted of spherical encapsulated PW, and the flow was controlled by forced convection. The rotating speed and size of the inner disk were shown to have a significant impact on flow dynamics and distinct flow zones. Changing the length of the inner disk had a greater impact on the dynamic characteristics of the liquid fraction than changing the height of the inner disk. According to this study, the introduction of a rotational feature can have a significant effect on the phase change dynamics. Shaker et al. [119] investigated the factors influencing the melting and solidification properties of a cylindrical encapsulated PCM. Solidification was simulated at an HTF temperature of 20–35 °C. Their findings showed that as the mean input water temperature increased, the melting time of lauric acid decreased. Under the same conditions, the melting time of PW was substantially longer than that of lauric acid. Additionally, increasing the number of fins inside the capsule from 0 to 12, at a mass water flow rate of 0.3238 kg s^{-1} and an intake temperature of 70°C, reduced the melting time of lauric acid by 37%. Rana et al. [120] used CFD simulation to optimize the design of rectangular tubes inside the shell and study the heat transport phenomena in PCM. The PCM used was a rectangular shell heat exchanger filled with gallium, and rectangular tubes were added for HTF flow. The influence of shape on heat transfer and PCM melting was investigated using two geometries of rectangular tubes: tubes without fins and tubes with four fins. Fins were placed around the circle of rectangular tubes, which were filled with hot temperature fluid. The fins inside the tubes enhanced heat transmission to the PCM and reduced the melting time of the PCM. By placing fins on each tube, the melting time of gallium was reduced from 301 to 290 s, resulting in an improved HTR from tubes to PCM. By incorporating fins into the tubes, the time for the PCM to reach the temperature of the water flowing through the tubes (800 °C) decreased from 460 to 425 s. Zhang et al. [121] investigated the melting process of encapsulated PCM through natural convection in six different capsule shapes and validated the obtained results with experimental data. CFD simulations were conducted to explore the effects of different inclination angles, temperature differences, and capsule sizes. The results revealed that the capsule shapes played a significant role in the phase change time. The short cylindrical capsule with a horizontal axis took the longest time (162 min), while the pyramidal capsule with a horizontal base had the shortest time (120 min). The tetrahedral and pyramidal capsules with a horizontal base melted more quickly than other shapes due to the increased heat transfer rate resulting from their larger surface areas. This research provides a validated model that can predict the dynamic melting of PCM with various geometries, enabling intelligent design of PCM panels for improved thermal management and comfort in buildings.

Rawat et al. [122] conducted a numerical investigation on the use of flanged fins to enhance the melting performance of PCM in a rectangular enclosure. The study explored the impact of fin length ratio, fin material, and the inclusion of flanged fins on the system's melting performance. The results indicated that a high PCM melting rate is achieved with a low fin length ratio and high thermal conductivity, with copper fins outperforming other materials. Additionally, placing a single flanged fin at the lower end of the container with a flanged-to-web ratio of 0.55 resulted in the minimum total melting time and cost per mean power.

Packed bed and porous media

Cascetta et al. [123] conducted a study on the performance of a sensible TESS utilizing a cylindrical-shaped carbon steel tank filled with spherical alumina beads for ES purposes. Air was used as the HTF, and alumina beads were chosen for their high thermal capacity and stability at high temperatures. The thermal behavior of the packed bed was approached by solving momentum, mass, and energy conservation equations. Additionally, the flow behavior of the system was determined by solving the unsteady Reynolds-averaged Navier–Stokes equations. Notably, separate energy equations were applied to the local thermal non-equilibrium model to simulate heat transfer in the porous medium. This approach was necessary due to significant differences in phase heat capacities and thermal conductivities. UDFs were utilized to define the HTC, effective thermal conductivity of phases, temperature value in the solid phase, and pressure drop in the porous bed. The simulations demonstrated that

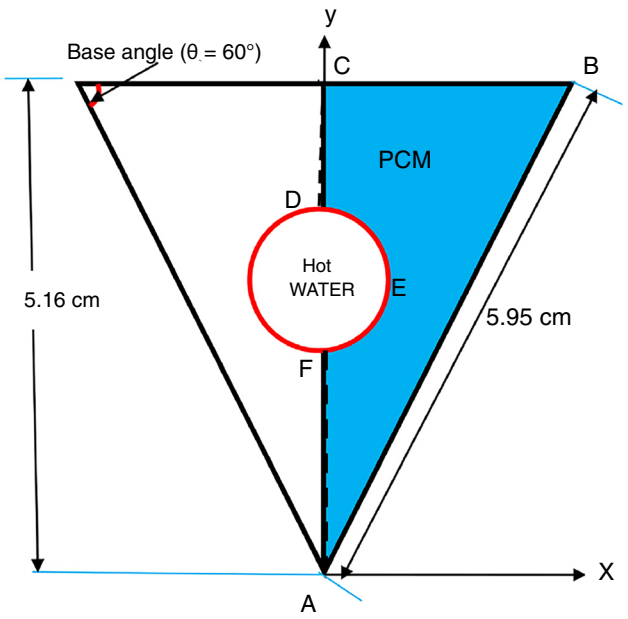

Fig. 13 Schematic cross-sectional view of an irregular-shaped double-pipe heat exchanger (The blue color region (Δ ABC) represents the simulation domain) presented by Tabassum et al. [113]

the pressure drop along the bed exhibited different behaviors during the melting and solidification processes. It increased during the charging phase and decreased during the discharging phase over time. Furthermore, it was shown that internal insulation of the common surface between the bed and the wall could enhance the thermal efficiency of the ESS.

In another study, Mousavi et al. [124] investigated the thermal performance of a photovoltaic/thermal system integrated with PCMs in a metal foam as a porous medium. They examined the effects of five different PCMs, including three organic (paraffin C18, paraffin C22, paraffin C15) and two inorganics (fatty acid, palmitic-capric acid), as well as sodium phosphate salt, to assess their impact on the system. The researchers highlighted the novelty and superiority of their research in using a metallic porous medium to enhance the low thermal conductivity of PCMs during phase change. Among the PCMs, the implementation of paraffin C22 resulted in the highest outlet water temperature, indicating better thermal efficiency. On the other hand, sodium phosphate salt exhibited the lowest absorber temperature, leading to improved electrical efficiency and high cooling performance. In contrast, palmitic/capric acid showed the opposite performance compared to salt. The authors emphasized that the porosity of the copper foam could have different effects on electrical and thermal efficiency, suggesting an optimum value for the metal foam. Overall, the efficiency of the system was influenced by factors such as melting temperature, enthalpy of fusion, and heat capacity.

Sardari et al. [125] investigated the charging process of a PCM-based TESS within a vertical square container filled with copper metal foam. They aimed to optimize the critical conditions that influence system performance and provide guidance for effective design to minimize waste energy in high-performance LHS units using porous metal foam-PCM composites. The chosen PCM for this study is RT-35 paraffin, selected for its lower melting temperature. To validate their code, the experimental data from studies conducted by Zhao et al. [125] and Tian et al. [126] were selected as references to validate the code. These references explored the melting process of RT-58 PCM with a porous medium inside a rectangular geometry, considering a heat flux boundary condition and free convection for the external walls. The presence of a large amount of liquid PCM is observed in the porous-PCM case, as heat transfer across the metal porous medium is primarily governed by conduction, which is more efficient. The study demonstrated that combining a low-porosity porous-PCM composite with a multiple-segment porous structure yields effective performance during the phase transformation process in LTES systems. Hu et al. [127] investigated the thermal performance of saturated PCM inside aluminum foam with a cubic periodic cell structure, which is considered an excellent candidate for the metal matrix of composites in TESS applications. In this study, PW R56-58 was used as the PCM. The cubic array of members in the 3D model of the aluminum matrix represented the ligament length and square cross section of the side, as depicted in Fig. 14. The study emphasized the importance of time in unsteady state numerical simulations. It was observed that the pore density and porosity of composite PCMs have distinct effects on melting time. Specifically, melting time increased with increase in porosity, while it decreased with increase in pore density. The utilization of PW inside the composite resulted in a more uniform temperature distribution compared to pure paraffin, leading to a reduction in melting time. The study confirmed that the heat exchange within the composite PCM during the melting process is enhanced by the convection heat transfer between the aluminum structure and paraffin. Figure 15 illustrates the phase distribution diagrams of the composite PCM. Furthermore, it was demonstrated that porosity values have an inverse relationship with effective thermal conductivity, whereas pore density has no effect on effective thermal conductivity when porosity remains the same. The study also highlighted the significant influence of the metal foam geometric structure on the thermal behavior of the composite PCM.

The thermal performance of a high-temperature rectangular packed-bed configuration TESS was investigated by Li et al. [128]. $NaLiCO_3$ (a eutectic salt) was used as PCM, whereas MgO and graphite flakes were exploited to enhance thermal conductivity. In addition, ferric oxide was

also used as a SHS substance to evaluate the thermal behavior of the PCM-based system. The researchers established a thermal exchange flow by introducing air as the HTF and PCM bricks to facilitate effective melting or solidification. The thermophysical properties and coefficients of PCM and HTF were incorporated into Fluent using UDF codes. It is worth mentioning that the effective heat capacity and density of the CPCM can be evaluated using the volume approach [129]. The Maxwell model was applied to calculate the effective thermal conductivity of the mentioned system [129, 130]. Due to the higher ES density of CPCMs, they require more heat and time compared to ferric oxide to complete the phase change process. However, the heat transfer efficiency of CPCMs is higher compared to ferric oxide-based systems. The results presented in this paper will contribute to expanding the applications of CPCMs-based high-temperature TESS and guide the optimization of structural designations. It should be noted that most organic and inorganic PCMs, such as salts or waxes, possess low thermal conductivity, which leads to low charging and discharging rates. This limitation affects thermal management efficiency and hampers their industrial applications. Therefore, extensive research has been conducted to improve the initial thermal characterizations of PCMs.

Porous media was utilized to boost the thermal conductivity of pure PCMs by many researchers owing to their tunable properties and effective heat dissipation capabilities [131]. Due to their high surface area-to-volume ratio and prolonged contact time, the amount of transferred heat is enhanced when this geometry configuration is applied. Among high-temperature LTES, packed bed is considered one of the most effective configurations for industrial and commercial applications [132]. Talebizadeh Sardari et al. [133] investigated the influence of enclosure size on LTES heat exchanger systems embedded in a porous medium. A 2D rectangular enclosure was considered as the computational domain. A PCM was embedded throughout a copper foam and heated by a constant flux from the bottom surface. Different configurations of the system were used to compare with a system without a porous medium. The thermal non-equilibrium model and the enthalpy–porosity approach were applied to evaluate the effects of the porous medium and phase change in the governing equations, respectively. The porous medium significantly increased the heat transfer value, but the enhancement of melting performance was highly dependent on the system's dimensions. By increasing the thermal diffusivity nearly 2.5 times compared to the PCM-only system, the porous medium had a stronger influence on the melting process in the solid-phase zone of the PCM. Furthermore, the effect of the porous medium on the melting duration was strongly dependent on the aspect ratio (width/height) of the storage systems. In the PCM-only system, the height had a larger influence than the width due to the contribution of natural convection in the free-flowing system. The melting time was reduced for the same storage capacity and total thermal energy quantity in the system with a lower height, particularly for the PCM-only system, due to the larger heat input area. When considering equal heat input, modifying the size of the storage system with the same dimensions resulted in a 7.4% reduction in melting time for the porous-PCM case and an 18.2% reduction for the PCM-only case. Mol et al. [134] investigated phase changes in unstructured packed beds as LTES into the open-source CFDEMR coupling application. Experimental data were used to validate the provided model. The validated model was employed to investigate the influence of system shape (e.g., employing numerous particle sizes and mixing multiple particle configurations) on the charging and discharging time the system of the PCM bed. It has been discovered that employing smaller particles results in quicker charging and discharging of the bed. By converting half of the bed into particles with half the diameter, a reduction of 26% was obtained. Furthermore, while fully charging the bed, it was discovered that adding tiny particles downstream had a greater influence on enhanced charging speed than placing them upstream. The configurations that were evaluated indicated a 20% reduction in charging time and a 13% reduction in discharging time. Because smaller particles undergo phase change faster than larger particles, the average temperature of the bed does not exhibit the flattening impact of phase shift as strongly. If heat flow is shut off before a particular threshold, the addition of smaller particles upstream can result in a higher charge rate and total charge. Mohammadnejad et al. [135] used CFD via COMSOL software to examine the discharging performance of a packed bed filled with high-temperature encapsulated PCMs layer by layer. The study revealed that increasing the input velocity of HTF and the porosity of the PCM layers in the packed bed had similar effects, resulting in a faster depletion of the packed bed. Several novel configurations were proposed, and their total energy consumption, defined as the proportion of the packed bed's total discharge time to the total time it took to receive energy at the optimum temperature, was improved. The results showed that arranging the layer heights of the PCMs in descending order and decreasing the porosity of each layer in the flow direction could lead to a 29.2% improvement in performance. Optimizing total energy usage can be a crucial factor in the design of packed beds and concentrating solar power plants. Comparing the data from five monitored heights revealed that the discharge process was completed more quickly when the PCMs were arranged in decreasing order. Conversely, a configuration with PCMs arranged in ascending order maintained the HTF at the desired temperature for a longer duration. Higher porosity coefficients and higher HTF input velocity resulted in a faster discharge process and less time for the HTF to leave the tank at the required temperature. Consequently,

the desired HTF temperature could be sustained for a longer period.

Packed-bed TESS have found extensive application across various fields due to their capacity and efficiency. The inherent flexibility of packed-bed systems allows for their utilization in diverse objectives, such as enhancing the thermal conductivity of PCMs and increasing HTR. To optimize the performance and efficiency of packed-bed systems, several key parameters must be considered. Research investigations have demonstrated that selecting an appropriate PCM, incorporating a metallic porous medium like metal foam, establishing a modified porous structure, designing precise geometric dimensions that account for process mechanisms, and implementing optimized operational conditions are crucial steps toward enhancing the performance of packed-bed systems. The porosity of the packed bed plays a vital role in improving the thermal storage efficiency. The use of porous media facilitates heat transfer between the HTF and PCM, resulting in improved phase change phenomena. It has been observed that the density of pores in the porous media significantly influences the melting time. However, the effective thermal conductivity is not affected by changes in porosity values. In addition to the utilization of porous media, careful consideration of the system geometry and design of the storage system with accurate dimensions, while taking into account heat transfer mechanisms, can greatly enhance system efficiency. For instance, the aspect ratio (width/height) of the storage system determines the degree of correlation between melting time and porosity. A summary of recent studies focusing on the geometric configurations of TESS is presented and illustrated in Table 2.

CFD simulations of advanced materials, additives, and novel PCMs

In the section on geometric configurations, it was observed that certain techniques, such as the incorporation of metal matrices or fin arrays, can enhance the heat transfer

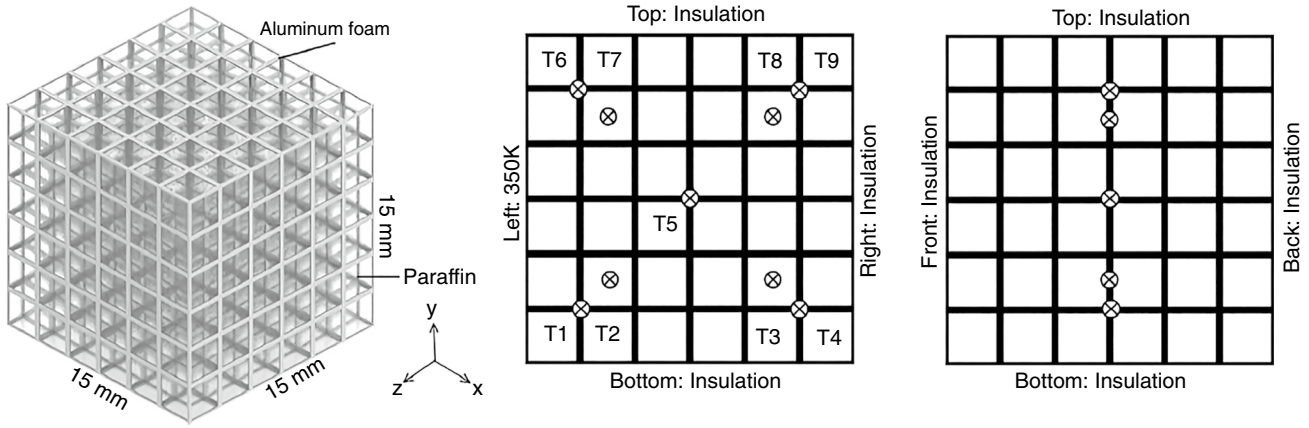

Fig. 14 Numerical model of aluminum foam/paraffin composite PCM in the unsteady state presented by Hu et al. [127]

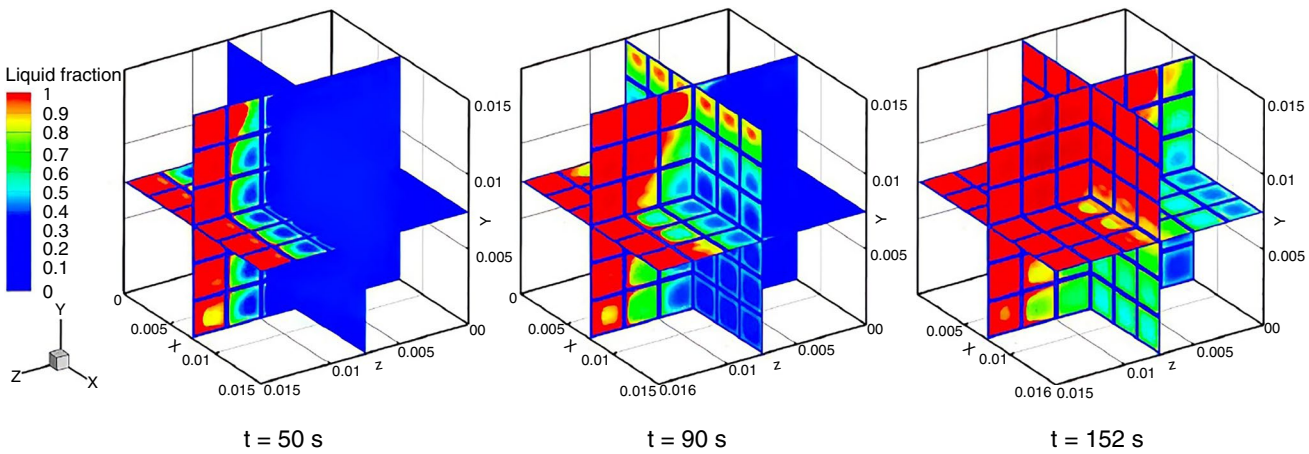

Fig. 15 Phase distribution diagrams of composite PCM at 30%, 50%, and 80% liquid fraction in the melting process presented by Hu et al. [127]

characteristics of TESS. These techniques promote greater convection effects to overcome the limited thermal conductivity exhibited by many types of PCMs. However, it should be noted that further geometrical adjustments may result in a reduced volume of available PCM, particularly in small-scale applications like electronic devices and lithium-ion batteries. To address these challenges, the integration of highly conductive additives and composite materials, such as nonadditive and porous metal foams, into PCMs has been explored. This approach not only enhances the thermophysical properties of PCMs but also allows for the adjustment of their melting and solidification ranges by varying the composition of the PCM/additive mixture, tailored to specific application requirements. The novel method to enhance the thermal features of PCMs is the use of various nanoadditives, including carbon-based nanoparticles (such as graphene, CNTs, graphene, and graphene oxide) [160, 161], metals and metal oxides (such as Ag, Al, Cu, TiO_2, SiO_2, and Al_2O_3 nanoparticles) [162–164], and composites (such as carbon-based/metal or metal oxides) [165]. This method improves the convection heat transfer of PCMs. Nanoadditives synthesis can be separated into two categories: top-down and bottom-up techniques. The top-down technique is considered a physical method that involves decomposing the mass of material into nanoparticles through approaches such as acid-etching [166], and ball-milling [167]. Conversely, the bottom-up technique relies on molecular precursors to form nanoparticles. This category includes co-precipitation [168], processes [169], microemulsion [170], and solvothermal [171] methods. Figure 16 illustrates different categories of commercial and advanced PCMs, as well as composite materials. One of the main challenges encountered when utilizing novel or modified materials as PCMs in CFD simulations is accurately defining their thermophysical properties. This challenge can be addressed through the use of UDFs, which enable the characterization and incorporation of these materials into the simulation framework. By employing UDFs, the thermal behavior and performance of such PCMs can be effectively evaluated.

In a numerical investigation, Koller et al. [5] used sodium nitrate wire matrix as the PCM in LTES. The results indicated that, initially, conduction was the only heat transfer mechanism during the melting process. However, as the melted region increased, natural convection became more significant, resulting in faster melting at the top of the storage device compared to the bottom. The use of the wire matrix method enhanced heat transfer, but certain assumptions were made to simplify the simulation. Therefore, in reality, higher contact resistance should be considered, leading to longer charging times and lower charging power compared to the simulation, which assumed ideal contact between the surfaces of the wires. Wang et al. [172] conducted experimental and numerical investigations to probe the performance of erythritol/HTF in a direct-contact ESS. The heat transfer mechanism and its relationship with the structure were examined using 2D CFD simulation. The PCM model was developed to evaluate the melting behavior of the PCM in the direct-contact storage unit, with the axial melting behavior difference neglected for simplification. The simulation results indicated a two-stage melting process. In the melting stage, vortexes and natural convection were observed in the liquid PCM region, leading to improved heat transfer. The solid PCM near the wall of the storage unit melted slowly due to low heat conduction, which dominated the solid PCM behavior. Increasing the flow rate resulted in higher ES efficiency. Kotze et al. [173] investigated eutectic aluminum–silicon alloy (AlSi12) used as PCM in concentrating solar power applications. To simplify the study, only discharge circumstances were examined for the direct steam generation idea, as the charge conditions need a CFD solution. For simplicity, the total volume of PCM was discretized into hexagonal cylinders surrounding each heat exchange pipe. FDM was employed by the authors who undertook analytical work on comparable Stefan issues to address the conduction problem, but it does not account for the solidification process at the solid–liquid interface [174]. An enthalpy tracking approach was used to tackle this problem. A heat transfer model of the moving boundary problem was presented to validate the concept and provide a foundation for comparing the simulation. This model was used to predict the performance of a large TESS. The results demonstrated reasonably matched trends, and further improvements can be achieved through increased materials testing and model development. An experimental investigation was conducted by Chen et al. [175] for a cold storage application. They absorbed dodecane into hydrophobic fumed silica and presented a stable CPCM. The schematic synthesis mechanism plus SEM images of the prepared PCM is demonstrated in Fig. 17. Numerical and experimental data for 75% and 85% composite PCM were compared. A slight difference between experimental and simulated results was observed due to the piecewise linear assumptions in all the thermal properties. Another reason for the high number of generated errors was the ignorance of the thermal contact resistance (TCR). They concluded that accurate thermophysical properties have the most critical effect on the solidification-melting simulations.

Abdollahzadeh et al. [176] numerically investigated Cu–water nanofluid inside a vertical enclosure as PCM. The effect of nanoparticle volume fraction on natural convection and solidification time variation with surface waviness was studied for different Grashof numbers. Solidification time was increased with geometrical patterns, especially by controlling surface waviness, which affects solidification mechanisms. The use of nanoparticles in PCMs decreased solidification time and also reduced the ES and release capacity in these materials.

Pure nitrates and shape-stabilized nitrate/EG composites thermal conductivities were investigated by Xiao et al. [177] using steady-state test equipment, considering the influence of TCR. These CPCMs were then encapsulated in a cylindrical LTES unit, and their thermal performance during the melting and solidification processes was examined both numerically and experimentally. The volume of fluid model was employed to describe the moving internal interface of the PCM–air system. The thermal conductivities were calculated based on steady-state assumptions, disregarding the effect of TCR on thermal conductivity. Images of the specimens with cold compression are shown in Fig. 18. The results demonstrated that the addition of EG to the nitrates significantly improved the thermal conductivities of the composite PCMs. For instance, the thermal conductivities of pure sodium composites were calculated to be approximately two, four, and seven times higher than that of pure sodium nitrate, respectively. It was observed that the thermal conductivities of nitrates and nitrate/EG composites decreased with increase in temperatures. The inclusion of EG in the nitrate/EG composite notably reduced the time required for heat storage and retrieval processes. The impact of EG on heat retrieval was more pronounced compared to heat storage. In the case of the pure binary nitrate system, natural convection dominated during heat storage, resulting in a gradually curved interface as the melting rate in the top section of the LTES unit was faster than that in the lower portion. During the melting process, the free surface of the liquid nitrate increased gradually due to the volume expansion, while during solidification, the free surface gradually decreased due to volume contraction. On the other hand, for the nitrate/EG composite, heat conduction played a dominant role in both heat storage and recovery processes. The high thermal conductivity of the nitrate/EG composite led to a reduced temperature gradient.

Mahdi et al. [178] numerically investigated the effects of nano-alumina (Al_2O_3) particle dispersion on the solidification performance of paraffin RT82 as a PCM. A triplex-tube TESS was applied as an ES medium in a solar-powered liquid-desiccant air-conditioning system. Under fixed HTF charging temperatures, a simulation of the complete solidification process was performed for diverse nanoparticle loadings. To take into account the temperature-dependent thermophysical characteristics of NEPCM, the UDF was programmed in C language. The computations were validated using their time-varying liquid fraction numerical results for the case without fins. They concluded that the inclusion of alumina nanoparticles enhances the thermal performance and accelerates the solidification of paraffin TR82. Low HTF charging temperature helps solidify components completely in a significantly shorter time, but it has no impact on the time saved by the addition of nanoparticles. Chen et al. [179] designed a quick charging tube-in-tank LTES system employing both the high thermal-conductive paraffin/EG composite and tiny spiral coil tubes. The effects of Re number, the ratio of the spiral coil tube helix radius to the radius of the PCM tank, the bulk density of the composite PCM, and as well as heat transfer temperature difference (HTTD), which is specified as the temperature discrepancy between the phase change temperature of utilized PCM and the HTF inlet temperature were investigated. The findings showed that raising Re or HTTD will result in a shorter TESS time. However, increasing Re and HTTD at the same time is not recommended due to the extra energy consumption of the pump or heat source. When developing a comparable LTES system, careful study and selection of Re and HTTD are required and Re should not be greater than 8700. Increasing the bulk density of paraffin/EG composite PCM results in increased latent TESS capacity and more crucially, decreased TESS time. Due to the high latent heat of the second phase shift peak, all temperature variation curves were stable for a long time at around 50 °C. Clearly, the concept of a phase change temperature ranges of 6 °C and the definition of heat capacity were reasonable since the general statistics of the temperature variation curves in the experiment and simulation are very similar. Alipanah et al. [180] investigated the TMS of lithium-ion batteries made from pure octadecane, pure gallium, and octadecane–Al foam. By using numerical approaches, metal foams were employed to improve the thermal properties of the PCM. The porosity of the Al foam varies between 0.97 and 0.925 and 0.88. The study's goal was to use numerical simulations to investigate the effective factors of the battery surface temperature, which impact performance and lifetime of batteries. On battery surface temperature, the impacts of TMS thickness, PCM characteristics, and the octadecane–Al metal foam composite were examined. By contrasting the surface temperature and uniformity of the battery utilizing pure octadecane, pure gallium, and octadecane-Al foam composite materials, the thermal effectivity of the TMS was evaluated. Due to the PCM's increased capacity for heat absorption, the battery with a thicker TMS had a longer discharge period before its average surface temperature exceeded 60 °C. The higher convective heat transfer was attributable to the worsening homogeneity of the battery surface temperature. Higher diffusivity results in a lower surface temperature and higher homogeneity. Compared to pure octadecane, TMSs made of gallium and octadecane-Al foam are better at storing battery waste heat. A metal matrix was added to the octadecane to improve the discharge period and significantly lower the battery surface temperature. Furthermore, because of the increased thermal conductivity and heat capacity of TMSs employing metal foams, the battery surface temperature was more uniform. The Al foam with

Table 2 Summarized CFD investigations of LTES systems incorporated PCMs for geometry section

References	Application	PCM	Geometry	Dimension	Discretization method	Numerical solution method	Assumption	Validation
Bouhal et al. [101]	TESS	Gallium	Cylindrical	2D	FEM	Physical enthalpy–porosity formulation	Symmetric melting of PCM Newtonian and incompressible flow Constant thermo-physical properties of PCM except density Boussinesq approximation Negligible viscous dissipation	–
Tay et al. [98]	TESS	Salt hydrate	Cylindrical	2D	–	Enthalpy method	Constant thermal resistance of PCM	Experimental
Hosseini et al. [95]	Heat exchanger	Paraffin RT50	Cylindrical	3D	FVM	Enthalpy–porosity method	Laminar, unsteady, and incompressible flow Boussinesq approximation The lateral surface of the outer tube is insulated	Agyenim et al. [136] And experimental
Jannesari et al. [99]	Heat exchanger	Water	Cylindrical	2D	FVM	Enthalpy method	Laminar and incompressible flow Newtonian behavior of PCM Constant thermal conductivities and specific heats Effects of viscous dissipation and radiation are neglected	Experimental

Table 2 (continued)

References	Application	PCM	Geometry	Dimension	Discretization method	Numerical solution method	Assumption	Validation
Kozak et al. [96]	Concentric storage unit	Eicosane ($C_{20}H_{42}$)	Cylindrical	2D	–	Enthalpy method	Laminar and quasi-steady flow in the thin molten liquid layer Natural convection, heat convection in the thin molten layer, and shear stresses on the solid bulk are neglected Constant properties of PCM	Experimental
Liu et al. [97]	Heat exchanger	Paraffin RT27	Cylindrical	2D	FVM	Enthalpy–porosity method	Natural convection occurs only in the cross sections but not along the axial direction	–
Lohrasbi et al. [100]	Heat exchanger (heat pipe)	Water	Cylindrical	2D	FEM	Enthalpy–porosity method	Conduction dominated solidification of PCM NEPCM is considered a continuous medium	Ismail et al. [137]
Ranjbaran et al. [138]	Lithium-ion battery	Paraffin RT27	Cylindrical	2D	–	Enthalpy–porosity method	Boussinesq approximation Negligible volume change during phase transient	Shmueli et al. [139]
Luo et al. [140]	Heat exchanger	Lauric acid	Cylindrical/fractal shaped	2D	–	Enthalpy–porosity method	Ignored natural convection for small densities of PCM Constant physical properties of PCM Constant wall temperature Adiabatic heat exchangers shell Ignored viscous dissipation effect	Nóbrega et al. [141]
Tay et al. [142]	TESS	Sodium nitrate	Rectangular/cylindrical	3D	–	–	–	Tay et al. [143]

Table 2 (continued)

References	Application	PCM	Geometry	Dimension	Discretization method	Numerical solution method	Assumption	Validation
Me et al. [144]	TESS	Paraffin wax	Rectangular/cylindrical	3D	–	Enthalpy–porosity method	Ignored thermal resistance of the heat exchanger Boussinesq approximation for natural convection Adiabatic rectangular storage unit's shell Uniform and homogeneous initial temperature inside the storage unit	Ma et al. [145]
Mousavi et al. [124]	Photovoltaic/thermal system	Fatty acid, palmitic-capric acid, Paraffin C18, C22 & C15	Rectangular cube/cylindrical tube	3D	FVM	–	Laminar, steady, and incompressible flow Neglected thickness of adhesive layer between the panel and absorber plate Neglected natural convection through the PCM	Browne et al. [146]
Ji et al. [106]	–	Paraffin RT42	Rectangular	2D	FVM	Enthalpy–porosity method	Boussinesq approximation	Kamkari et al. [147]
Prieto et al. [104]	Heat exchanger	Paraffin RT60 & palmitic acid	Rectangular	2D	FVM	Enthalpy–porosity method	Constant initial temperature in the PCM domain	Shokouhmand et al. [148], Hosseini et al. [95]
Zhou et al. [105]	Solar thermal system	Sodium thiosulfate ($Na_2S_2O_3{\cdot}5H_2O$)	Rectangular cube	3D	FVM	Multiphase Method (UDF)	Neglected radiation heat transfer Constant thermophysical properties of PCM	Chen et al. [149]

Table 2 (continued)

References	Application	PCM	Geometry	Dimension	Discretization method	Numerical solution method	Assumption	Validation
Hu et al. [127]	TSS	PW R56-58	Rectangular cube / square	3D	FVM	Enthalpy–porosity method	Laminar and incompressible flow Boussinesq approximation Negligible radiation heat transfer Constant, homogeneous, and isotropic PCM and aluminum foam	Xu et al. [150]
Ying et al. [151]	LTES	Paraffin/Cu foam	Rectangular (Cu filled in PCM)	2D	FVM	Enthalpy–porosity method	Incompressible and laminar flow of liquid PCM Boussinesq approximation (for buoyancy effect) Isotropic PCM and metal foam Constant thermophysical properties of PCM and Cu foam	Zheng et al. [152]
Rawat et al. [153]	Heat exchanger	RT42	Rectangular/T-shaped	2D	FVM	Enthalpy–porosity method	Unsteady state flow during melting process Laminar, Newtonian, and incompressible liquid PCM flow Constant thermophysical properties of PCM Ignored volumetric changes of PCM during phase change Neglected radiation heat transfer Boussinesq approximation to model buoyancy force-driven natural convection	Ji et al. [106]

Table 2 (continued)

References	Application	PCM	Geometry	Dimension	Discretization method	Numerical solution method	Assumption	Validation
Kumaresan et al. [154]	Solar thermal system	D-Mannitol & oil	Spherical/annular	3D	FVM	Enthalpy–porosity method	Constant density, specific heat, and thermal conductivity of the HTF The insulated outer surface of the cooling unit	Experimental
Tripathi et al. [155]	TSS/solar heating system	PW, Sodium acetate trihydrate & Lauric acid	Spherical	2D	FVM	Enthalpy–porosity method	Unsteady state heat transfer condition existence Homogeneous and isotropic PCM The insulated outer wall of the sphere	-
Kumarasamy et al. [156]	TSS	*n*-Octadecane	Spherical/cylindrical	3D	–	Enthalpy–temperature method	Pure, homogeneous, and isotropic PCM material Temperature independent thermophysical properties of the PCM and shell	Experimental
Lin et al. [157]	–	*n*-Octadecane	Spherical	2D	FVM	Enthalpy method	Unsteady and incompressible liquid PCM Homogeneous and isotropic phases Constant thermophysical properties for the PCM in all phases Ignored densities between solid and liquid phases Constant temperature around the spheres	Experimental

Table 2 (continued)

References	Application	PCM	Geometry	Dimension	Discretization method	Numerical solution method	Assumption	Validation
Tabassum et al. [113]	Heat exchanger	PW	Cylindrical, elliptical, prolated & Triangular-shaped	2D	Control-volume finite difference CVFD	Enthalpy–porosity method	Simulation with a fixed coordinate system Laminar flow of melted phase Incompressible and Newtonian fluid Ignored viscous dissipation Ignored heat loss or heat gain from the surroundings	Yazici et al. [158]
Elsayed et al. [114]	Solar heating system	PW	Triangular-shaped	2D	FVM	Enthalpy–porosity method	Laminar, steady, and incompressible flow Constant thermophysical properties of PCM Fixed solid phase of PCM	Ali et al. [159]
Sardari et al. [125]	TSS	Paraffin RT35	Square tank (Rectangular cube)	3D	FVM	Enthalpy–porosity method	Incompressible and Newtonian fluid Boussinesq approximation Homogeneous and isotropic porous medium Negligible volume expansion during phase transient Neglected viscous dissipation	Zhao et al. [125], Tian et al. [126]

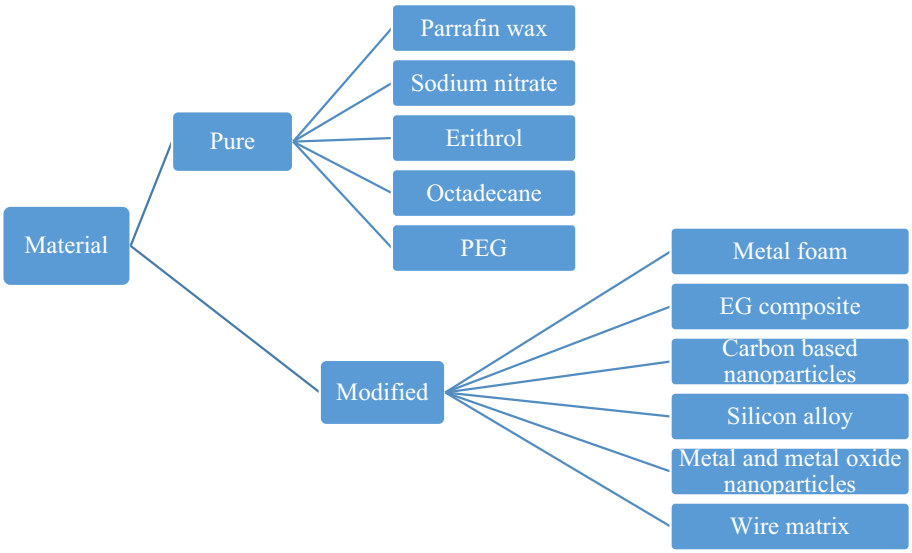

Fig. 16 Various classes of PCMs reported in literature

a porosity of 0.88 was preferred among the foam materials which investigated, because it produces a lower surface temperature and greater homogeneity. The decreased flow motion results in greater homogeneity of the battery surface temperature. Parsazadeh et al. [9] conducted a CFD evaluation on a shell and tube TESS unit made from a common organic PCM, PW. Nanoparticles of Al_2O_3 were dispersed in the PCM. A CFD model was developed to study the melting of the PCM with the following parameters: nanoparticle concentration of 0 to 4 vol%; fin angle (α) from – 45° to 45°, and pitch (p) from 45 to 65 mm. In this investigation, the Al_2O_3 concentration ranges from 0 (pure PCM) to 4 vol%, because larger nanoparticle concentrations would not enhance the overall HTR and could cause the model to be inaccurate [10]. The results revealed that at an early stage of heat transmission, when the liquid percentage was 0.25, heat conduction was dominating, and melting occurred only along the HTF tube's wall. At this point, the investigated factors (fin angle, nanoparticle concentration, and pitch) had slightly influenced the melting process. In all cases studied, adding Al_2O_3 nanoadditives into the PW declined the thermal performance resulting in a longer charging time in all cases. Their results indicated that thermal conductivity improvement with nanoadditives may not be able to make up for natural convection reduction when the nanoadditives are added to the finned TESS unit. In another study, Othman et al. [181] investigated the CuO NP's impacts on the solidification time of a unit with curved walls filled with water. Results illustrated that dispersing nanoparticles can accelerate the solidification process, and the NP's shape affects the conductivity of the mixture. The FEM was used to solve the energy equation, and the results demonstrated that the increase in the fraction of nanoparticles and shape factor can significantly decrease the solidification time. Furthermore, the using of nanoparticles can improve the performance of storage systems. When the fraction of CuO nanoparticles increases from zero to 0.04, the required solidification time decreases by 31.39%.

The thermal conductivity of the PCMs was enhanced by the use of a high porosity metal foam, resulting in enhanced heat transfer and, hence, promoting the PCM melting and

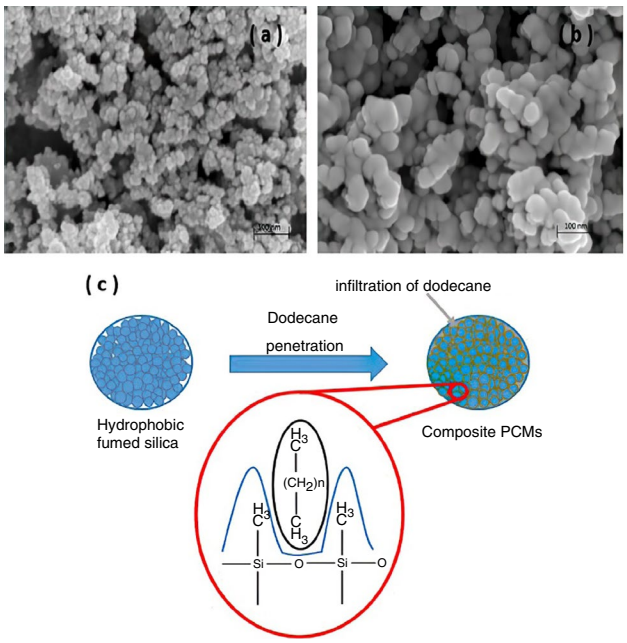

Fig. 17 **a** SEM image of the fumed silica, **b** SEM image of dodecane/hydrophobic fumed silica composite PCM with 85 mass% dodecane and **c** schematic diagram of the synthesis mechanism presented by Chen et al. [175]

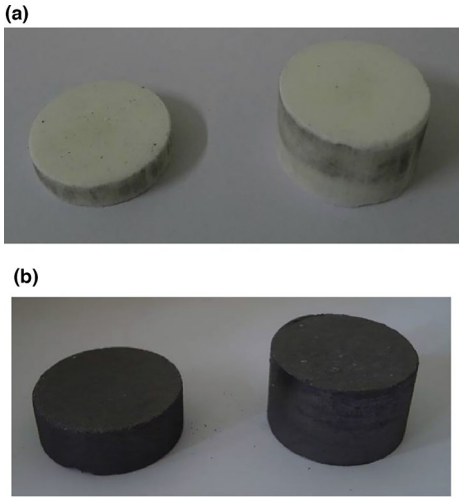

Fig. 18 Pictures of the specimens with cold compression **a** $NaNO_3$, **b** $NaNO_3$/5 mass% EG presented by Xiao et al. [177]

solidification by Alhusseny et al. [182]. An open-cell copper foam filled with PCM, specifically PW, is incorporated into staggered bundled tubes to create a TESS. The schematic representation of this design is depicted in Fig. 19. The PCM unit is charged and discharged by utilizing moderately hot- and cold-water streams that pass through the tube-bundle units. The proposed design of the LTES system was found to be not only easy to configure but also highly efficient, exhibiting remarkable overall performance. Moreover, by carefully selecting the design parameters, the charging and discharging rates can be significantly increased, surpassing those of similar methods using pure paraffin by more than 50%. The combination of PCM-metal foam composites into a LTES system offers exciting prospects due to the vast surface area available for heat exchange in bundled tube architectures and the exceptional potential of such composites. The results indicate that the solidification process takes approximately half the time required for a similar system to melt, primarily due to the significant role of buoyancy during the early stages of these processes. Furthermore, it was discovered that denser storage units outperform lighter systems in terms of storage capacity density and charging or discharging time. Table 3 provides a summary and illustration of recent CFD studies focusing on the material configurations of TESS.

Conclusions

TESS integration with PCMs has emerged as a viable and environmentally friendly approach to maximizing energy efficiency and reducing reliance on fossil fuels. This study extensively reviews the application of PCMs in various

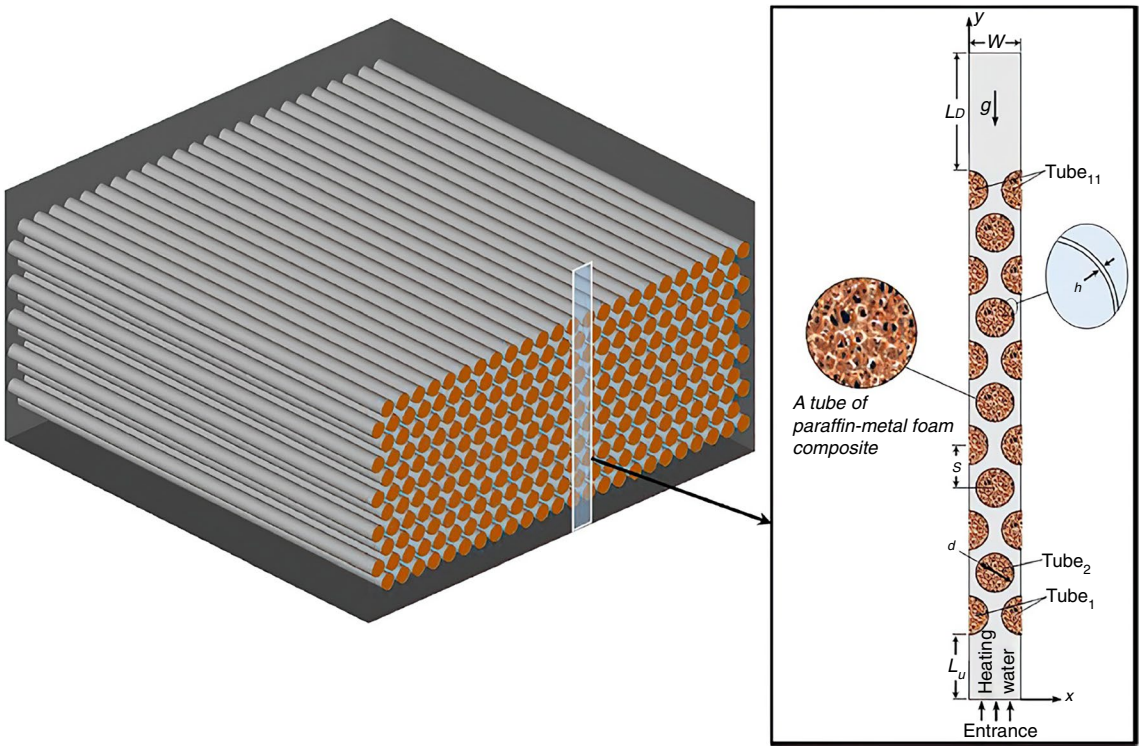

Fig. 19 Schematic description of the LTES unit examined presented by Alhusseny et al. [182]

Table 3 Summarized CFD investigations of LTES systems incorporated PCMs for materials section

References	Application	PCM	Geometry	Dimension	Discretization method	Numerical solution method	Assumption	Validation
Chen et al. [175]	Cold TESS (food industries)	Dodecane/dodecane-SiO_2 composite	Cubic cell (rectangular)/square	2D	FEM	Enthalpy method	Constant density of CM in all phases Negligible TCR Extreme viscosity of PCM composite	Experimental
Chen et al. [179]	TSS	Paraffin/paraffin-expanded graphite composite	Spiral coil tube (cylindrical)	3D	FVM	Heat capacity method	Constant physical properties of water Constant heat capacity and thermal conductivities of composite PCM Adiabatic boundaries outside the composite PCM and straight tube	Experimental
Zeneli et al. [183]	Ultra-high TSS (Photovoltaic thermal system)	Silicon	Frustum-shaped/spherical/cylindrical/cubic (square)	2D & 3D	FVM	Enthalpy–porosity method	No additional gap between the walls and PCM Asymmetric problem solving (symmetric shapes)	Assis et al. [184]
Zheng et al. [185]	Photovoltaic thermal system	Silica aerogel/CPCM	Rectangular cube/cylindrical tube	3D	FVM	Enthalpy–porosity method	Neglected contact thermal resistance Laminar, incompressible and fully developed cooling medium flows Isotropic and homogeneous materials Ignored subcooling phenomenon Neglected volume expansion during phase transition process Neglected reflection of solar radiation	Zhao et al. [186], Browne et al. [146], Su et al. [187]

Table 3 (continued)

References	Application	PCM	Geometry	Dimension	Discretization method	Numerical solution method	Assumption	Validation
Xiao et al. [177]	TSS	Nitrate binary mixtures/expanded graphite composite (Encapsulated)	Cylindrical (cone shape)	2D	FVM	Enthalpy–porosity method	The binary nitrate is isotropic and homogeneous Melting and solidification processes are axisymmetric Incompressible and Newtonian liquid binary nitrate and laminar flow of convection Negligible surface tension	Experimental
Parsazadeh et al. [10]	TSS	NEOCM (CuO-paraffin)	Cylindrical	2D	FVM	Enthalpy–porosity method	The uniform flow of nanofluid inside the tube Negligible thermal resistance between NEPCM and HTF Symmetry boundary condition of the shell and tube System	Sciacovelli et al. [74], Aydin et al. [188]
Wang et al. [172]	TSS, heat exchanger	Erythritol (HTO)	Cylindrical	2D	FVM	Enthalpy–porosity method	Convective laminar and Newtonian flow Ignoring the melting behavior difference in the axial direction	Experimental

Table 3 (continued)

References	Application	PCM	Geometry	Dimension	Discretization method	Numerical solution method	Assumption	Validation
Momeni et al. [189]	Heat exchanger	Docosane	Complex geometry	3D	FEM	Enthalpy–porosity method	Incompressible, Newtonian, and isotropic liquid phases Constant thermophysical properties of air, water, and PCM Laminar water flow, and turbulent airflow Uniform and homogeneous mass of PCM Uniform initial temperature of domains Neglected radiation heat transfer	Fotowat et al. [190]
Kong et al. [191]	Water ESS	Sodium acetate trihydrate/water	Spherical, cylindrical	1D & 2D	FDM	Enthalpy method	Same temperature of PCM in one layer Uniform flow distribution in the flow direction inside the energy storage Neglected volume of the metallic structure	Experimental
Parsazadeh et al. [9]	Solar & wind ESS	PW with Al_2O_3 nanoparticle	Cylindrical	2D	FVM	Enthalpy–porosity method	Boussinesq approximation	Sciacovelli et al. [192]

Table 3 (continued)

References	Application	PCM	Geometry	Dimension	Discretization method	Numerical solution method	Assumption	Validation
Shakibi et al. [193]	Solar energy collector	RT27/Cu NPs	Rectangular	3D	–	Enthalpy–porosity method	Monotonous solar irradiance, solar cell layer properties, and temperature dispensation Homogeneous PCM layer in both solid and liquid phases Negligible thermal resistance of the layers between the PV cell layer and the PCM layer Uniform, incompressible, and fully developed fluid of the finned-tube collector	Khanjari et al.[194], Selmi et al. [195]
Mahdi et al. [178]	TSS	Al_2O_3 NPs incorporated Paraffin RT82	Cylindrical/annulus	2D	FVM	Enthalpy–porosity method	Laminar, transient, and incompressible flow Negligible temperature variation in the HTF Negligible viscous dissipation Constant thermophysical properties of PCM except density	Al-Abidi et al. [196]
Rostami Dibavar et al. [21]	–	NEPCM (water-ferrooxide NPs)	Annulus	2D	FVM	Enthalpy–porosity method	Laminar, steady and incompressible flow Constant thermophysical properties of PCM except density Boussinesq approximation	Darzi et al. [197]

Table 3 (continued)

References	Application	PCM	Geometry	Dimension	Discretization method	Numerical solution method	Assumption	Validation
Samimi et al. [198]	Lithium-ion battery	Paraffin mixtures/carbon fiber-PCM composite	Cylindrical/rectangular	3D	FVM	–	Boussinesq approximation The effective thermal conductivity dependence on fiber mass fractions and temperature subjected to the Brownian motion	Experimental
Anter et al. [199]	Energy efficient buildings	RT27/RT31/RT42/RT35HC/RT44HC/lauric acid	Rectangular	2D	–	Enthalpy–porosity method	Isotropic thermophysical characteristics of phases Ignored thermal resistance of the examined layers Fully inserted PCM into the PCM cavity	Experimental
Sun et al. [200]	Energy efficient buildings	TM24/EP & TM24/EG inorganic composites	Rectangular	1D	FDM	Enthalpy method	Not mentioned	Velsco et al. [201], Ramakrishnan et al. [202], Guarino et al. [203]
Jin et al. [204]	Building façade	Organic paraffin wax/thermochromic glazing unit	Rectangular	2D	FVM	Enthalpy–porosity method	One-dimensional unsteady heat transfer process through the glazing units Thermally homogeneous and isotropic materials Considered surfaces of the glazing systems as diffuse gray surface Adiabatic edges of the glazing systems Uniform incident irradiation applying to exterior surface	Gowreesunker et al. [205]

industrial settings, including building compartments, lithium-ion batteries, solar energy systems (SE), heating and cooling systems, and electronic devices. The following interpretations are highlighted by this investigation:

- Notably, the passive implementation of TESS plays a crucial role in safeguarding on-board applications such as electric vehicles (EVs), by preventing thermal runaways and nail penetrations in lithium-ion batteries, as well as mitigating malfunctions in electronic devices like smartphones. Computational fluid dynamics (CFD) simulations enable the prediction of TESS's thermal characteristics and the determination of optimal geometrical configurations for PCM containers and layer thicknesses.
- SE systems and building compartments integrated with TESS have been extensively investigated due to the need for efficient energy storage and release during periods of limited SE availability, such as nighttime. The selection of PCM melting and solidification ranges should be carefully considered, given the diverse climates worldwide and seasonal variations. Numerical techniques facilitate the identification of appropriate PCMs with minimal operational costs and effort.
- In heating and cooling applications, which have been extensively explored using CFD simulations, conventional organic PCMs with low thermal conductivity require geometrical modifications, such as the inclusion of fins and extended surfaces, to enhance convective heat transfer. Furthermore, packed-bed and porous media configurations have emerged as promising approaches for improving heat transfer between the heat transfer fluid (HTF) and PCM, leading to more efficient phase change phenomena. Porosity and pore density are crucial parameters in CFD investigations involving porous media, as they significantly impact melting time.
- While CFD simulations have confirmed the efficacy of geometrical adjustments in addressing the limited thermal behavior of organic PCMs, their application in small-scale systems remains constrained by the limitations of further surface extensions. Consequently, the literature introduces PCM composites with modified thermophysical properties achieved through the incorporation of metal foams and alloys, conductive nanoparticles, and ethylene glycol (EG). To explore and optimize the modified thermophysical properties of PCM composites, CFD simulations in conjunction with user-defined functions (UDFs) can be employed. These simulations enable researchers to investigate the thermal behavior of novel synthesized PCMs and determine the desired mass fractions of the additive materials. By utilizing CFD simulations and UDFs, researchers can accurately model and predict the thermal characteristics of the PCM composites, assisting in the design and optimization of small-scale systems.

Future perspectives and limitations

As mentioned previously, PCMs play a crucial role in optimizing energy consumption. With the long-term energy shortage that humanity is expected to face, there is a need for further scrutiny of novel materials to meet future energy demands. Numerical simulation and modeling are valuable tools for predicting various processes, offering advantages in terms of cost and time savings. Therefore, this study focused on utilizing CFD methods in PCM technology, addressing a gap in the existing literature. The review comprehensively covered various PCM applications, geometries, and materials, providing detailed discussions on each topic. Optimal methods and devices were introduced to guide future studies in employing appropriate simulation techniques for PCM research. However, it is important to acknowledge that new hybrid materials and applications are constantly being discovered. Therefore, this review can serve as a foundation for future research to select the best PCM materials and efficient geometries for various desired applications. Furthermore, it is important to note that CFD simulations may encounter limitations in complex processes or geometries, including convergence issues and high computational resource requirements. Future investigations could focus on simulating hybrid nanomaterials in complex and combined geometries to achieve notable efficiency and overcome the aforementioned limitations of the CFD method.

Author contributions The contribution of all authors to the manuscript is the same.

Funding The present research received no funding.

Data availability All data generated or analyzed during this study are included in this published article.

Declarations

Conflict of interest The authors declare that they have no conflict of interest.

References

1. Azimi B, Tahmasebpoor M, Sanchez-Jimenez PE, Perejon A, Valverde JM. Multicycle CO_2 capture activity and fluidizability of Al-based synthesized CaO sorbents. Chem Eng J. 2019;358:679–90.
2. Tahmasebpoor M, Iranvandi M, Heidari M, Azimi B, Pevida C. Development of novel waste tea-derived activated carbon

promoted with SiO_2 nanoparticles as highly robust and easily fluidizable sorbent for low-temperature CO_2 capture. J Environ Chem Eng. 2023;11(5):110437.
3. Iranvandi M, Tahmasebpoor M, Azimi B, Heidari M, Pevida C. The novel SiO_2-decorated highly robust waste-derived activated carbon with homogeneous fluidity for the CO_2 capture process. Sep Purif Technol. 2023;306: 122625.
4. Ray AK, Rakshit D, Kumar KR, Gurgenci H. Strength-Weakness-Opportunities-Threats-Unusual (SWOT-U) behavior analysis of silicon as phase change material for high-temperature latent heat storage. Thermal Sci Eng Progr. 2023;38: 101627.
5. Koller M, Walter H, Hameter M. Transient numerical simulation of the melting behavior of $NaNO_3$ in a latent thermal energy storage device using a wire matrix for enhancing the heat transfer. Energies. 2016;9:9–17.
6. Dabiri S, Mehrpooya M, Nezhad EG. Latent and sensible heat analysis of PCM incorporated in a brick for cold and hot climatic conditions, utilizing computational fluid dynamics. Energy. 2018;159:160–71.
7. Greco A, Jiang X. A coupled thermal and electrochemical study of lithium-ion battery cooled by paraffin/porous-graphite-matrix composite. J Power Sources. 2016;315:127–39.
8. Moghadam AV, Goshayeshi HR, Chaer I, Paurine A, Zeinali Heris S, Pourpasha H. Experimental investigation of multiwall carbon nanotubes/water nanofluid pool boiling on smooth and groove surfaces. Int J Energy Res. 2022;46(14):19882–93.
9. Parsazadeh M, Duan X. Numerical study on the effects of fins and nanoparticles in a shell and tube phase change thermal energy storage unit. Appl Energy. 2018;216:142–56.
10. Parsazadeh M, Duan X. Numerical and statistical study on melting of nanoparticle enhanced phase change material in a shell-and-tube thermal energy storage system. Appl Therm Eng. 2017;111:950–60.
11. Pourpasha H, Heris SZ, Mohammadpourfard M. The effect of TiO_2 doped multi-walled carbon nanotubes synthesis on the thermophysical and heat transfer properties of transformer oil: a comprehensive experimental study. Case Stud Thermal Eng. 2023;41: 102607.
12. Hou Y, Qiu J, Wang W, He X, Ayyub M, Shuai Y. Preparation and performance improvement of chlorides/MgO ceramics shape-stabilized phase change materials with expanded graphite for thermal energy storage system. Appl Energy. 2022;316: 119116.
13. Wang T, Tseng K, Zhao J. Development of efficient air-cooling strategies for lithium-ion battery module based on empirical heat source model. Appl Therm Eng. 2015;90:521–9.
14. Pourpasha H, Mohammadfam Y, Khani L, Mohammadpourfard M, Heris SZ. Thermodynamic and thermoeconomic analyses of a new dual-loop organic Rankine-Generator absorber heat exchanger power and cooling cogeneration system. Energy Convers Manage. 2020;224: 113356.
15. Sharifi N, Bergman TL, Allen MJ, Faghri A. Melting and solidification enhancement using a combined heat pipe, foil approach. Int J Heat Mass Transf. 2014;78:930–41.
16. Sunku Prasad J, Anandalakshmi R, Muthukumar P. Numerical investigation on conventional and PCM heat sinks under constant and variable heat flux conditions. Clean Technol Environ Policy. 2021;23(4):1105–20.
17. Alizadeh H, Pourpasha H, Heris SZ, Estellé P. Experimental investigation on thermal performance of covalently functionalized hydroxylated and non-covalently functionalized multi-walled carbon nanotubes/transformer oil nanofluid. Case Stud Thermal Eng. 2022;31: 101713.
18. Zeinelabdein R, Omer S, Mohamed E. Parametric study of a sustainable cooling system integrating phase change material energy storage for buildings. J Energy Storage. 2020;32: 101972.
19. Pourpasha H, Farshad P, Heris SZ. Modeling and optimization the effective parameters of nanofluid heat transfer performance using artificial neural network and genetic algorithm method. Energy Rep. 2021;7:8447–64.
20. Xu H, Romagnoli A, Sze JY, Py X. Application of material assessment methodology in latent heat thermal energy storage for waste heat recovery. Appl Energy. 2017;187:281–90.
21. Dibavar MR, Mohammadpourfard M, Mohseni F, Heris SZ. Numerical study on the effect of non-uniform magnetic fields on melting and solidification characteristics of NEPCMs in an annulus enclosure. Energy Convers Manage. 2018;171:879–89.
22. Zauner C, Hengstberger F, Etzel M, Lager D, Hofmann R, Walter H. Experimental characterization and simulation of a fin-tube latent heat storage using high density polyethylene as PCM. Appl Energy. 2016;179:237–46.
23. Sarier N, Onder E. Organic phase change materials and their textile applications: an overview. Thermochim Acta. 2012;540:7–60.
24. Fornarelli F, Camporeale SM, Fortunato B, Torresi M, Oresta P. CFD analysis of melting process in a shell-and-tube latent heat storage for concentrated solar power plants. Appl Energy. 2016;164:711–22.
25. Dutil Y, Rousse DR, Salah NB, Lassue S, Zalewski L. A review on phase-change materials: mathematical modeling and simulations. Renew Sustain Energy Rev. 2011;15(1):112–30.
26. Al-Abidi AA, Mat SB, Sopian K, Sulaiman M, Mohammed AT. CFD applications for latent heat thermal energy storage: a review. Renew Sustain Energy Rev. 2013;20:353–63.
27. Voller VR, Prakash C. A fixed grid numerical modelling methodology for convection-diffusion mushy region phase-change problems. Int J Heat Mass Transf. 1987;30(8):1709–19.
28. Karimi Shoar Z, Pourpasha H, Zeinali Heris S, Mousavi SB, Mohammadpourfard M. The effect of heat transfer characteristics of macromolecule fouling on heat exchanger surface: a dynamic simulation study. Can J Chem Eng. 2023. https://doi.org/10.1002/cjce.24832.
29. Gowreesunker B, Tassou S. Effectiveness of CFD simulation for the performance prediction of phase change building boards in the thermal environment control of indoor spaces. Build Environ. 2013;59:612–25.
30. Iten M, Liu S, Shukla A. Experimental validation of an air-PCM storage unit comparing the effective heat capacity and enthalpy methods through CFD simulations. Energy. 2018;155:495–503.
31. Brent A, Voller VR, Reid K. Enthalpy-porosity technique for modeling convection-diffusion phase change: application to the melting of a pure metal. Numer Heat Transfer, Part A Appl. 1988;13(3):297–318.
32. Li Y, Nord N, Xiao Q, Tereshchenko T. Building heating applications with phase change material: a comprehensive review. J Energy Storage. 2020;31: 101634.
33. Kumar A, Tiwari AK, Said Z. A comprehensive review analysis on advances of evacuated tube solar collector using nanofluids and PCM. Sustain Energy Technol Assess. 2021;47: 101417.
34. Nejat P, Jomehzadeh F, Taheri MM, Gohari M, Majid MZA. A global review of energy consumption, CO_2 emissions and policy in the residential sector (with an overview of the top ten CO_2 emitting countries). Renew Sustain Energy Rev. 2015;43:843–62.
35. Yu J, Yang H, Tao J, Zhao J, Luo Y. Performance evaluation and optimum design of ventilation roofs with different positions of shape-stabilized PCM. Sustainability. 2023;15(11):8721.
36. Bhamare DK, Rathod MK, Banerjee J. Numerical model for evaluating thermal performance of residential building roof

integrated with inclined phase change material (PCM) layer. J Build Eng. 2020;28: 101018.
37. Zhang Y, Du K, He J, Yang L, Li Y. Impact factors analysis of the enthalpy method and the effective heat capacity method on the transient nonlinear heat transfer in phase change materials (PCMs). Numer Heat Transfer, Part A: Appl. 2014;65(1):66–83.
38. Tokuç A, Başaran T, Yesügey SC. An experimental and numerical investigation on the use of phase change materials in building elements: the case of a flat roof in Istanbul. Energy Build. 2015;102:91–104.
39. Diarce G, Campos-Celador Á, Martin K, Urresti A, García-Romero A, Sala J. A comparative study of the CFD modeling of a ventilated active façade including phase change materials. Appl Energy. 2014;126:307–17.
40. Khattari Y, Arid A, El Ouali A, Kousksou T, Janajreh I. CFD study on the validity of using PCM in a controlled cooling ceiling integrated in a ventilated room. Develop Built Environ. 2022;9: 100066.
41. Wang C. A numerical study on applying the movable PCM design to disaster-relief prefabricated temporary houses used in different climate regions to improve indoor thermal environments in summer. Int J Energy Res. 2022;46(14):20401–14.
42. Hendricks C, Williard N, Mathew S, Pecht M. A failure modes, mechanisms, and effects analysis (FMMEA) of lithium-ion batteries. J Power Sources. 2015;297:113–20.
43. Chen K, Song M, Wei W, Wang S. Design of the structure of battery pack in parallel air-cooled battery thermal management system for cooling efficiency improvement. Int J Heat Mass Transf. 2019;132:309–21.
44. Huo Y, Rao Z, Liu X, Zhao J. Investigation of power battery thermal management by using mini-channel cold plate. Energy Convers Manage. 2015;89:387–95.
45. Karimi D, Behi H, Van Mierlo J, Berecibar M. Novel hybrid thermal management system for high-power lithium-ion module for electric vehicles: fast charging applications. World Electric Vehicle J. 2022;13(5):86.
46. Sun Z, Fan R, Yan F, Zhou T, Zheng N. Thermal management of the lithium-ion battery by the composite PCM-Fin structures. Int J Heat Mass Transf. 2019;145: 118739.
47. Qian Z, Li Y, Rao Z. Thermal performance of lithium-ion battery thermal management system by using mini-channel cooling. Energy Convers Manage. 2016;126:622–31.
48. Verma A, Shashidhara S, Rakshit D. A comparative study on battery thermal management using phase change material (PCM). Thermal Sci Eng Progr. 2019;11:74–83.
49. Ling Z, Chen J, Fang X, Zhang Z, Xu T, Gao X, Wang S. Experimental and numerical investigation of the application of phase change materials in a simulative power batteries thermal management system. Appl Energy. 2014;121:104–13.
50. Kshetrimayum KS, Yoon YG, Gye HR, Lee CJ. Preventing heat propagation and thermal runaway in electric vehicle battery modules using integrated PCM and micro-channel plate cooling system. Appl Therm Eng. 2019;159: 113797.
51. Bernardi D, Pawlikowski E, Newman J. A general energy balance for battery systems. J Electrochem Soc. 1985;132(1):5.
52. Zhao R, Liu J, Gu J. Simulation and experimental study on lithium ion battery short circuit. Appl Energy. 2016;173:29–39.
53. An Z, Chen X, Zhao L, Gao Z. Numerical investigation on integrated thermal management for a lithium-ion battery module with a composite phase change material and liquid cooling. Appl Therm Eng. 2019;163: 114345.
54. Xin Q, Xiao J, Yang T, Zhang H, Long X. Thermal management of lithium-ion batteries under high ambient temperature and rapid discharging using composite PCM and liquid cooling. Appl Therm Eng. 2022;210: 118230.
55. Kargaran M, Goshayeshi HR, Pourpasha H, Chaer I, Heris SZ. An extensive review on the latest developments of using oscillating heat pipe on cooling of photovoltaic thermal system. Thermal Sci Eng Progr. 2022;36:101489.
56. Elsheniti MB, Hemedah MA, Sorour M, El-Maghlany WM. Novel enhanced conduction model for predicting performance of a PV panel cooled by PCM. Energy Convers Manage. 2020;205: 112456.
57. Chaabane M, Mhiri H, Bournot P. Thermal performance of an integrated collector storage solar water heater (ICSSWH) with phase change materials (PCM). Energy Convers Manage. 2014;78:897–903.
58. Raj A, Srinivas M, Jayaraj S. CFD modeling of macro-encapsulated latent heat storage system used for solar heating applications. Int J Therm Sci. 2019;139:88–104.
59. Bashir MA, Giovannelli A. Design optimization of the phase change material integrated solar receiver: a numerical parametric study. Appl Therm Eng. 2019;160: 114008.
60. Modest MF. Chapter 23-inverse radiative heat transfer. In: Radiative heat transfer. Amsterdam: Elsevier; 2013. p. 779–802.
61. Ramana A, Venkatesh R, Raj VAA, Velraj R. Experimental investigation of the LHS system and comparison of the stratification performance with the SHS system using CFD simulation. Sol Energy. 2014;103:378–89.
62. Iranmanesh M, Akhijahani HS, Jahromi MSB. CFD modeling and evaluation the performance of a solar cabinet dryer equipped with evacuated tube solar collector and thermal storage system. Renew Energy. 2020;145:1192–213.
63. Al-Najjar HMT, Mahdi JM. Novel mathematical modeling, performance analysis, and design charts for the typical hybrid photovoltaic/phase-change material (PV/PCM) system. Appl Energy. 2022;315: 119027.
64. Pavithran A, Sharma M, Shukla AK. An investigation on the effect of PCM incorporation in refrigerator through CFD simulation. Mater Today: Proceed. 2021;46:5555–64.
65. Zarajabad OG, Ahmadi R. Numerical investigation of different PCM volume on cold thermal energy storage system. J Energy Storage. 2018;17:515–24.
66. Marques A, Davies G, Maidment G, Evans J, Wood I. Novel design and performance enhancement of domestic refrigerators with thermal storage. Appl Therm Eng. 2014;63(2):511–9.
67. Elarem R, Mellouli S, Abhilash E, Jemni A. Performance analysis of a household refrigerator integrating a PCM heat exchanger. Appl Therm Eng. 2017;125:1320–33.
68. Ezan MA, Doganay EO, Yavuz FE, Tavman IH. A numerical study on the usage of phase change material (PCM) to prolong compressor off period in a beverage cooler. Energy Convers Manage. 2017;142:95–106.
69. Copertaro B, Principi P, Fioretti R. Thermal performance analysis of PCM in refrigerated container envelopes in the Italian context–Numerical modeling and validation. Appl Therm Eng. 2016;102:873–81.
70. Hu Y, Heiselberg PK, Drivsholm C, Søvsø AS, Vogler-Finck PJ, Kronby K. Experimental and numerical study of PCM storage integrated with HVAC system for energy flexibility. Energy Build. 2022;255: 111651.
71. Arshad A, Jabbal M, Yan Y. Preparation and characteristics evaluation of mono and hybrid nano-enhanced phase change materials (NePCMs) for thermal management of microelectronics. Energy Convers Manage. 2020;205: 112444.
72. Kurhade A, Talele V, Rao TV, Chandak A, Mathew V. Computational study of PCM cooling for electronic circuit of smartphone. Mater Today: Proceed. 2021;47:3171–6.
73. Alshaer W, Nada S, Rady M, Le Bot C, Del Barrio EP. Numerical investigations of using carbon foam/PCM/Nano carbon tubes

composites in thermal management of electronic equipment. Energy Convers Manage. 2015;89:873–84.
74. Huang Z, Xie N, Zheng X, Gao X, Fang X, Fang Y, Zhang Z. Experimental and numerical study on thermal performance of Wood's alloy/expanded graphite composite phase change material for temperature control of electronic devices. Int J Therm Sci. 2019;135:375–85.
75. Tomizawa Y, Sasaki K, Kuroda A, Takeda R, Kaito Y. Experimental and numerical study on phase change material (PCM) for thermal management of mobile devices. Appl Therm Eng. 2016;98:320–9.
76. Arshad A, Jabbal M, Sardari PT, Bashir MA, Faraji H, Yan Y. Transient simulation of finned heat sinks embedded with PCM for electronics cooling. Thermal Sci Eng Progr. 2020;18: 100520.
77. Ghadikolaei S, Siahchehrehghadikolaei S, Gholinia M, Rahimi M. A CFD modeling of heat transfer between CGNPs/H_2O Eco-friendly nanofluid and the novel nature-based designs heat sink: hybrid passive techniques for CPU cooling. Thermal Sci Eng Progr. 2023;37: 101604.
78. Alqallaf HJ, Alawadhi EM. Concrete roof with cylindrical holes containing PCM to reduce the heat gain. Energy Build. 2013;61:73–80.
79. Essid N, Eddhahak A, Neji J. Experimental and numerical analysis of the energy efficiency of PCM concrete wallboards under different thermal scenarios. J Build Eng. 2022;45: 103547.
80. Wang P, Liu Z, Xi S, Zhang Y, Zhang L. Experiment and numerical simulation of an adaptive building roof combining variable transparency shape-stabilized PCM. Energy Build. 2022;263: 112030.
81. Zhao L, Xing Y, Wang Z, Liu X. The passive thermal management system for electronic device using low-melting-point alloy as phase change material. Appl Therm Eng. 2017;125:317–27.
82. Youssef W, Ge Y, Tassou S. CFD modelling development and experimental validation of a phase change material (PCM) heat exchanger with spiral-wired tubes. Energy Convers Manage. 2018;157:498–510.
83. Bonamente E, Aquino A, Cotana F. A PCM thermal storage for ground-source heat pumps: simulating the system performance via CFD approach. Energy Procedia. 2016;101:1079–86.
84. Peng P, Wang Y, Jiang F. Numerical study of PCM thermal behavior of a novel PCM-heat pipe combined system for Li-ion battery thermal management. Appl Therm Eng. 2022;209: 118293.
85. Javani N, Dincer I, Naterer G, Rohrauer G. Modeling of passive thermal management for electric vehicle battery packs with PCM between cells. Appl Therm Eng. 2014;73(1):307–16.
86. Kizilel R, Sabbah R, Selman JR, Al-Hallaj S. An alternative cooling system to enhance the safety of Li-ion battery packs. J Power Sources. 2009;194(2):1105–12.
87. Wang Z, Zhang H, Xia X. Experimental investigation on the thermal behavior of cylindrical battery with composite paraffin and fin structure. Int J Heat Mass Transf. 2017;109:958–70.
88. Javani N, Dincer I, Naterer G, Yilbas B. Heat transfer and thermal management with PCMs in a Li-ion battery cell for electric vehicles. Int J Heat Mass Transf. 2014;72:690–703.
89. Chaouachi B, Gabsi S. Experimental study of integrated collector storage solar water heater under real conditions. Renew Energy Rev. 2006;9(2):75–82.
90. Trp A. An experimental and numerical investigation of heat transfer during technical grade paraffin melting and solidification in a shell-and-tube latent thermal energy storage unit. Sol Energy. 2005;79(6):648–60.
91. Muhammad M, Badr O, Yeung H. Validation of a CFD melting and solidification model for phase change in vertical cylinders. Numer Heat Transfer, Part A: Appl. 2015;68(5):501–11.
92. Karami M, Shahini N, Behabadi MAA. Numerical investigation of double-walled direct absorption evacuated tube solar collector using microencapsulated PCM and nanofluid. J Mol Liq. 2023;377: 121560.
93. Zolfalizadeh M, Zeinali Heris S, Pourpasha H, Mohammadpourfard M, Meyer JP. Experimental investigation of the effect of graphene/water nanofluid on the heat transfer of a shell-and-tube heat exchanger. Int J Energy Res. 2023;2023:1–16.
94. Bondareva NS, Sheremet MA. 3D natural convection melting in a cubical cavity with a heat source. Int J Therm Sci. 2017;115:43–53.
95. Hosseini M, Rahimi M, Bahrampoury R. Experimental and computational evolution of a shell and tube heat exchanger as a PCM thermal storage system. Int Commun Heat Mass Transfer. 2014;50:128–36.
96. Kozak Y, Rozenfeld T, Ziskind G. Close-contact melting in vertical annular enclosures with a non-isothermal base: theoretical modeling and application to thermal storage. Int J Heat Mass Transf. 2014;72:114–27.
97. Liu H, Li S, Chen Y, Sun Z. The melting of phase change material in a cylinder shell with hierarchical heat sink array. Appl Therm Eng. 2014;73(1):975–83.
98. Tay N, Belusko M, Castell A, Cabeza LF, Bruno F. An effectiveness-NTU technique for characterising a finned tubes PCM system using a CFD model. Appl Energy. 2014;131:377–85.
99. Jannesari H, Abdollahi N. Experimental and numerical study of thin ring and annular fin effects on improving the ice formation in ice-on-coil thermal storage systems. Appl Energy. 2017;189:369–84.
100. Lohrasbi S, Miry SZ, Gorji-Bandpy M, Ganji DD. Performance enhancement of finned heat pipe assisted latent heat thermal energy storage system in the presence of nano-enhanced H_2O as phase change material. Int J Hydrog Energy. 2017;42(10):6526–46.
101. Bouhal T, Kousksou T, Jamil A. CFD thermal energy storage enhancement of PCM filling a cylindrical cavity equipped with submerged heating sources. J Energy Storage. 2018;18:360–70.
102. Soodmand AM, Nejatbakhsh S, Pourpasha H, Aghdasinia H, Heris SZ. Simulation of melting and solidification process of polyethylene glycol 1500 as a PCM in rectangular, triangular, and cylindrical enclosures. Alex Eng J. 2022;61(11):8431–56.
103. Zhu M, Nan W, Wang Y. Analysis on the thermal behaviour of the latent heat storage system using S-CO_2 and H-PCM. Renew Energy. 2023;208:240–50.
104. Prieto M, González B. Fluid flow and heat transfer in PCM panels arranged vertically and horizontally for application in heating systems. Renew Energy. 2016;97:331–43.
105. Zhou G, Han Y. Numerical simulation on thermal characteristics of supercooled salt hydrate PCM for energy storage: Multiphase model. Appl Therm Eng. 2017;125:145–52.
106. Ji C, Qin Z, Dubey S, Choo FH, Duan F. Simulation on PCM melting enhancement with double-fin length arrangements in a rectangular enclosure induced by natural convection. Int J Heat Mass Transf. 2018;127:255–65.
107. Zhao C, Wang J, Sun Y, He S, Hooman K. Fin design optimization to enhance PCM melting rate inside a rectangular enclosure. Appl Energy. 2022;321: 119368.
108. Arévalo R, Antúnez D, Rebollo L, Abánades A. Estimation of radiation coupling factors in film boiling around spheres by mean of computational fluid dynamics (CFD) tools. Int J Heat Mass Transf. 2014;78:84–9.
109. Amin N, Bruno F, Belusko M. Effective thermal conductivity for melting in PCM encapsulated in a sphere. Appl Energy. 2014;122:280–7.

110. Tay N, Bruno F, Belusko M. Experimental validation of a CFD model for tubes in a phase change thermal energy storage system. Int J Heat Mass Transf. 2012;55(4):574–85.
111. Aziz S, Amin N, Majid MA, Belusko M, Bruno F. CFD simulation of a TES tank comprising a PCM encapsulated in sphere with heat transfer enhancement. Appl Therm Eng. 2018;143:1085–92.
112. Cofré-Toledo J, Roa-Cossio D, Vasco DA, Cabeza LF, Rouault F. Numerical simulation of the melting and solidification processes of two organic phase change materials in spherical enclosures for cold thermal energy storage applications. J Energy Storage. 2022;51: 104337.
113. Tabassum T, Hasan M, Begum L. 2-D numerical investigation of melting of an impure PCM in the arbitrary-shaped annuli. Int J Therm Sci. 2017;114:296–319.
114. Elsayed AO. Numerical investigation on PCM melting in triangular cylinders. Alex Eng J. 2018;57(4):2819–28.
115. Saxena A, Goel V. Solar air heaters with thermal heat storages. Chinese J Eng. 2013;2013:11.
116. Kasibhatla R, Brüggemann D. Coupled conjugate heat transfer model for melting of PCM in cylindrical capsules. Appl Therm Eng. 2021;184: 116301.
117. Kasibhatla RR, König-Haagen A, Rösler F, Brüggemann D. Numerical modelling of melting and settling of an encapsulated PCM using variable viscosity. Heat Mass Transf. 2017;53(5):1735–44.
118. Selimefendigil F, Öztop HF, Doranehgard MH, Karimi N. Phase change dynamics in a cylinder containing hybrid nanofluid and phase change material subjected to a rotating inner disk. J Energy Storage. 2021;42: 103007.
119. Shaker MY, Sultan AA, El Negiry EA, Radwan A. Melting and solidification characteristics of cylindrical encapsulated phase change materials. J Energy Storage. 2021;43: 103104.
120. Rana S, Zunaid M, Kumar R. CFD simulation for heat transfer enhancement in phase change materials. Mater Today: Proceed. 2021;46:10915–21.
121. Zhang Y, Bozorg MV, Torres JF, Zhao Y, Wang X. Dynamic melting of encapsulated PCM in various geometries driven by natural convection of surrounding air: a modelling-based parametric study. J Energy Storage. 2022;48: 103975.
122. Rawat P, Sherwani AF. A numerical study on the impact of fin length arrangement and material on the melting of PCM in a rectangular enclosure. Int J Heat Mass Transf. 2023;205: 123932.
123. Cascetta M, Cau G, Puddu P, Serra F. A comparison between CFD simulation and experimental investigation of a packed-bed thermal energy storage system. Appl Therm Eng. 2016;98:1263–72.
124. Mousavi S, Kasaeian A, Shafii MB, Jahangir MH. Numerical investigation of the effects of a copper foam filled with phase change materials in a water-cooled photovoltaic/thermal system. Energy Convers Manage. 2018;163:187–95.
125. Sardari PT, Mohammed HI, Giddings D, Gillott M, Grant D. Numerical study of a multiple-segment metal foam-PCM latent heat storage unit: effect of porosity, pore density and location of heat source. Energy. 2019;189: 116108.
126. Tian Y, Zhao C-Y. A numerical investigation of heat transfer in phase change materials (PCMs) embedded in porous metals. Energy. 2011;36(9):5539–46.
127. Hu X, Gong X. Pore-scale numerical simulation of the thermal performance for phase change material embedded in metal foam with cubic periodic cell structure. Appl Therm Eng. 2019;151:231–9.
128. Li C, Li Q, Ding Y. Investigation on the thermal performance of a high temperature packed bed thermal energy storage system containing carbonate salt based composite phase change materials. Appl Energy. 2019;247:374–88.
129. Chan KC, Chao CY. A theoretical model on the effective stagnant thermal conductivity of an adsorbent embedded with a highly thermal conductive material. Int J Heat Mass Transf. 2013;65:863–72.
130. Li C, Li Q, Cao H, Leng G, Li Y, Wang L, Zheng L, Ding Y. Wettability of eutectic $NaLiCO_3$ salt on magnesium oxide substrates at 778 K. Appl Surf Sci. 2018;442:148–55.
131. Esence T, Bruch A, Molina S, Stutz B, Fourmigué J-F. A review on experience feedback and numerical modeling of packed-bed thermal energy storage systems. Sol Energy. 2017;153:628–54.
132. Oró E, Castell A, Chiu J, Martin V, Cabeza LF. Stratification analysis in packed bed thermal energy storage systems. Appl Energy. 2013;109:476–87.
133. Talebizadeh Sardari P, Walker GS, Gillott M, Grant D, Giddings D. Numerical modelling of phase change material melting process embedded in porous media: effect of heat storage size. Proceed Instit Mech Eng, Part A: J Power Energy. 2020;234(3):365–83.
134. Mol J, Shahi M, Mahmoudi A. Numerical modeling of thermal storage performance of encapsulated PCM particles in an unstructured packed bed. Energies. 2020;13(23):6413.
135. Mohammadnejad F, Hossainpour S. A CFD modeling and investigation of a packed bed of high temperature phase change materials (PCMs) with different layer configurations. J Energy Storage. 2020;28: 101209.
136. Agyenim F, Eames P, Smyth M. A comparison of heat transfer enhancement in a medium temperature thermal energy storage heat exchanger using fins. Sol Energy. 2009;83(9):1509–20.
137. Ismail K, Alves C, Modesto M. Numerical and experimental study on the solidification of PCM around a vertical axially finned isothermal cylinder. Appl Therm Eng. 2001;21(1):53–77.
138. Ranjbaran YS, Haghparast SJ, Shojaeefard M, Molaeimanesh G. Numerical evaluation of a thermal management system consisting PCM and porous metal foam for Li-ion batteries. J Therm Anal Calorim. 2020;141(5):1717–39.
139. Shmueli H, Ziskind G, Letan R. Melting in a vertical cylindrical tube: numerical investigation and comparison with experiments. Int J Heat Mass Transf. 2010;53(19–20):4082–91.
140. Luo X, Gu J, Ma H, Xie Y, Li A, Wang J, Ding R. Numerical study on enhanced melting heat transfer of PCM by the combined fractal fins. J Energy Storage. 2022;45: 103780.
141. Nóbrega CR, Ismail KA, Lino FA. Enhancement of ice formation around vertical finned tubes for cold storage applications. Int J Refrig. 2019;99:251–63.
142. Tay N, Belusko M, Liu M, Bruno F. Investigation of the effect of dynamic melting in a tube-in-tank PCM system using a CFD model. Appl Energy. 2015;137:738–47.
143. Tay N, Bruno F, Belusko M. Experimental validation of a CFD and an ε-NTU model for a large tube-in-tank PCM system. Int J Heat Mass Transf. 2012;55(21–22):5931–40.
144. Ma Y, Tao Y, Shi L, Wang Y, Tu J. Natural convection and structural impact of rectangular PCM storage units through the modular expansion. J Energy Storage. 2023;68: 107781.
145. Ma Y, Tao Y, Shi L, Wang Y, Tu J, Wang L. Thermal performance improvement of a low-temperature thermal energy storage with configuration optimization. J Energy Storage. 2023;60: 106620.
146. Browne MC, Norton B, McCormack SJ. Heat retention of a photovoltaic/thermal collector with PCM. Sol Energy. 2016;133:533–48.
147. Kamkari B, Shokouhmand H, Bruno F. Experimental investigation of the effect of inclination angle on convection-driven melting of phase change material in a rectangular enclosure. Int J Heat Mass Transf. 2014;72:186–200.

148. Shokouhmand H, Kamkari B. Experimental investigation on melting heat transfer characteristics of lauric acid in a rectangular thermal storage unit. Exp Thermal Fluid Sci. 2013;50:201–12.
149. Chen SL, Lee TS. A study of supercooling phenomenon and freezing probability of water inside horizontal cylinders. Int J Heat Mass Transf. 1998;41(4–5):769–83.
150. Xu WQ, Yuan XG, Li Z. Study on effective thermal conductivity of metal foam matrix composite phase change materials. J Funct Mater. 2009;8(10):1329–37.
151. Ying Q, Wang H, Lichtfouse E. Numerical simulation on thermal behavior of partially filled metal foam composite phase change materials. Appl Therm Eng. 2023;229: 120573.
152. Zheng ZJ, Yang C, Xu Y, Cai X. Effect of metal foam with two-dimensional porosity gradient on melting behavior in a rectangular cavity. Renew Energy. 2021;172:802–15.
153. Rawat P, Goyal A, Sherwani AF. A comparative numerical study about the impact of rectangular and T shaped fins on melting of PCM in a rectangular enclosure. Appl Therm Eng. 2023;228: 120461.
154. Kumaresan G, Raju G, Iniyan S, Velraj R. CFD analysis of flow and geometric parameter for a double walled solar cooking unit. Appl Math Model. 2015;39(1):137–46.
155. Tripathi S, Tomar A. CFD Analysis and Melting Performance of PCMs in two dimensional sphere. Int Res J Eng Technol. 2017;4(7):3350–8.
156. Kumarasamy K, An J, Yang J, Yang E-H. Novel CFD-based numerical schemes for conduction dominant encapsulated phase change materials (EPCM) with temperature hysteresis for thermal energy storage applications. Energy. 2017;132:31–40.
157. Lin Q, Wang S, Ma Z, Wang J, Zhang T. Lattice Boltzmann simulation of flow and heat transfer evolution inside encapsulated phase change materials due to natural convection melting. Chem Eng Sci. 2018;189:154–64.
158. Yazici MY, Avci M, Aydin O, Akgun M. On the effect of eccentricity of a horizontal tube-in-shell storage unit on solidification of a PCM. Appl Therm Eng. 2014;64(1–2):1–9.
159. Ali M, Zeitoun O, Nuhait A. Forced convection heat transfer over horizontal triangular cylinder in cross flow. Int J Therm Sci. 2011;50(1):106–14.
160. Pourpasha H, Zeinali Heris S, Mohammadfam Y. Comparison between multi-walled carbon nanotubes and titanium dioxide nanoparticles as additives on performance of turbine meter oil nano lubricant. Scient Rep. 2021;11(1):11064.
161. Liu J, Chen Z, Liu Y, Liu Z, Ren Y, Xue Y, Zhu B, Wang R, Zhang Q. Preparation of a PCM microcapsule with a graphene oxide platelet-patched shell and its thermal camouflage applications. Ind Eng Chem Res. 2019;58(41):19090–9.
162. Nejatbakhsh S, Aghdasinia H, Ebrahimi Farshchi M, Azimi B, Karimi A. Adsorptive desulfurization of liquid hydrocarbons utilizing granular Cu/Cr-BDC@ γ-Al_2O_3 bimetal-organic frameworks. Ind Eng Chem Res. 2022;61(32):11617–27.
163. Khataee A, Farshchi ME, Fathinia M, Aghdasinia H. Photocatalytic ozonation process for degradation of an anthelmintic drug using ceramic coated TiO_2 NPs: CFD simulation coupling with kinetic mechanisms. Process Saf Environ Prot. 2020;141:37–48.
164. Ehsani A, Aghdasinia H, Farshchi ME, Rostamnia S, Khataee A. Synthesis of sodium alginate/carboxy-methyl cellulose/Cu-based metal-organic framework composite for adsorption of tetracycline from aqueous solution: isotherm, kinetic and thermodynamic approach. Surf Interfaces. 2023;36: 102506.
165. Ebrahimi Farshchi M, Aghdasinia H, Rostamnia S, Sillanpää M (2023) Catalytic adsorptive elimination of deleterious contaminant in a pilot fluidised-bed reactor by granulated Fe_3O_4/Cu-MOF/cellulose nanocomposites: RSM optimisation and CFD approach. Int J Environ Analyt Chem, pp. 1–22. https://doi.org/10.1080/03067319.2023.2170752
166. Miao W, Gan S, Li X, Lv Y. A triply synergistic method for palygorskite activation to effectively impregnate phase change materials (PCMs) for thermal energy storage. Appl Clay Sci. 2020;189: 105530.
167. Yang L, Zhang N, Yuan Y, Cao X, Xiang B. Thermal performance of stearic acid/carbon nanotube composite phase change materials for energy storage prepared by ball milling. Int J Energy Res. 2019;43(12):6327–36.
168. Yan T, Li Z, Pan W. 3D network structural shape-stabilized composite PCMs for integrated enhancement of thermal conductivity and photothermal properties. Sol Energy Mater Sol Cells. 2022;240: 111645.
169. Latibari ST, Mehrali M, Mehrali M, Mahlia TMI, Metselaar HSC. Synthesis, characterization and thermal properties of nanoencapsulated phase change materials via sol–gel method. Energy. 2013;61:664–72.
170. Sarkar S, Mestry S, Mhaske S. Developments in phase change material (PCM) doped energy efficient polyurethane (PU) foam for perishable food cold-storage applications: a review. J Energy Storage. 2022;50: 104620.
171. Ehsani A, Nejatbakhsh S, Soodmand AM, Farshchi ME, Aghdasinia H. High-performance catalytic reduction of 4-nitrophenol to 4-aminophenol using M-BDC (M= Ag Co, Cr, Mn, and Zr) metal-organic frameworks. Environ Res. 2023;227: 115736.
172. Wang W, He S, Guo S, Yan J, Ding J. A combined experimental and simulation study on charging process of Erythritol–HTO direct-blending based energy storage system. Energy Convers Manage. 2014;83:306–13.
173. Kotzé JP, Von Backström T, Erens P. Simulation and testing of a latent heat thermal energy storage unit with metallic phase change material. Energy Procedia. 2014;49:860–9.
174. Hoshi A, Mills DR, Bittar A, Saitoh TS. Screening of high melting point phase change materials (PCM) in solar thermal concentrating technology based on CLFR. Sol Energy. 2005;79(3):332–9.
175. Chen J, Ling Z, Fang X, Zhang Z. Experimental and numerical investigation of form-stable dodecane/hydrophobic fumed silica composite phase change materials for cold energy storage. Energy Convers Manage. 2015;105:817–25.
176. Abdollahzadeh M, Esmaeilpour M. Enhancement of phase change material (PCM) based latent heat storage system with nano fluid and wavy surface. Int J Heat Mass Transf. 2015;80:376–85.
177. Xiao X, Zhang P, Li M. Experimental and numerical study of heat transfer performance of nitrate/expanded graphite composite PCM for solar energy storage. Energy Convers Manage. 2015;105:272–84.
178. Mahdi JM, Nsofor EC. Solidification of a PCM with nanoparticles in triplex-tube thermal energy storage system. Appl Therm Eng. 2016;108:596–604.
179. Chen C, Zhang H, Gao X, Xu T, Fang Y, Zhang Z. Numerical and experimental investigation on latent thermal energy storage system with spiral coil tube and paraffin/expanded graphite composite PCM. Energy Convers Manage. 2016;126:889–97.
180. Alipanah M, Li X. Numerical studies of lithium-ion battery thermal management systems using phase change materials and metal foams. Int J Heat Mass Transf. 2016;102:1159–68.
181. Othman HA, Rguigui H, Altoum SH, Elamin MA. Nanomaterial efficacy on freezing of PCM with involvement of numerical simulation. J Mol Liq. 2022;362: 119658.
182. Alhusseny A, Al-Zurfi N, Nasser A, Al-Fatlawi A, Aljanabi M. Impact of using a PCM-metal foam composite on charging/discharging process of bundled-tube LHTES units. Int J Heat Mass Transf. 2020;150: 119320.

183. Zeneli M, et al. Numerical simulation of a silicon-based latent heat thermal energy storage system operating at ultra-high temperatures. Appl Energy. 2019;242:837–53.
184. Assis E, Katsman L, Ziskind G, Letan R. Numerical and experimental study of melting in a spherical shell. Int J Heat Mass Transf. 2007;50(9–10):1790–804.
185. Zheng X, Zhou Y. A three-dimensional unsteady numerical model on a novel aerogel-based PV/T-PCM system with dynamic heat-transfer mechanism and solar energy harvesting analysis. Appl Energy. 2023;338: 120899.
186. Zhao L, Bhatia B, Yang S, Strobach E, Weinstein LA, Cooper TA, Chen G, Wang EN. Harnessing heat beyond 200 C from unconcentrated sunlight with nonevacuated transparent aerogels. ACS Nano. 2019;13(7):7508–16.
187. Su D, Jia Y, Lin Y, Fang G. Maximizing the energy output of a photovoltaic–thermal solar collector incorporating phase change materials. Energy Build. 2017;153:382–91.
188. Aydın O, Akgün M, Kaygusuz K. An experimental optimization study on a tube-in-shell latent heat storage. Int J Energy Res. 2007;31(3):274–87.
189. Momeni M, Fartaj A. Numerical thermal performance analysis of a PCM-to-air and liquid heat exchanger implementing latent heat thermal energy storage. J Energy Storage. 2023;58: 106363.
190. Fotowat S, Askar S, Fartaj A. Experimental transient response of a minichannel heat exchanger with step flow variation. Exp Thermal Fluid Sci. 2017;89:128–39.
191. Kong W, Wang G, Englmair G, Nielsen ENN, Dragsted J, Furbo S, Fan J. A simplified numerical model of PCM water energy storage. J Energy Storage. 2022;55: 105425.
192. Sciacovelli A, Colella F, Verda V. Melting of PCM in a thermal energy storage unit: numerical investigation and effect of nanoparticle enhancement. Int J Energy Res. 2013;37(13):1610–23.
193. Shakibi H, Shokri A, Sobhani B, Yari M. Numerical analysis and optimization of a novel photovoltaic thermal solar unit improved by Nano-PCM as an energy storage media and finned collector. Renew Sustain Energy Rev. 2023;179: 113230.
194. Khanjari Y, Kasaeian A, Pourfayaz F. Evaluating the environmental parameters affecting the performance of photovoltaic thermal system using nanofluid. Appl Therm Eng. 2017;115:178–87.
195. Selmi M, Al-Khawaja MJ, Marafia A. Validation of CFD simulation for flat plate solar energy collector. Renew Energy. 2008;33(3):383–7.
196. Al-Abidi AA, Mat S, Sopian K, Sulaiman M, Mohammad AT. Numerical study of PCM solidification in a triplex tube heat exchanger with internal and external fins. Int J Heat Mass Transf. 2013;61:684–95.
197. Darzi AR, Farhadi M, Sedighi K. Numerical study of melting inside concentric and eccentric horizontal annulus. Appl Math Model. 2012;36(9):4080–6.
198. Samimi F, Babapoor A, Azizi M, Karimi G. Thermal management analysis of a Li-ion battery cell using phase change material loaded with carbon fibers. Energy. 2016;96:355–71.
199. Anter AG, Sultan AA, Hegazi A, El Bouz M. Thermal performance and energy saving using phase change materials (PCM) integrated in building walls. J Energy Storage. 2023;67: 107568.
200. Sun W, Zhang Z, Wu Z, Xu Y. Numerical modeling and optimization of annual thermal characteristics of an office room with PCM active–passive coupling system. Energy Build. 2022;254: 111629.
201. Tabares-Velasco PC, Christensen C, Bianchi M. Verification and validation of EnergyPlus phase change material model for opaque wall assemblies. Build Environ. 2012;54:186–96.
202. Ramakrishnan S, Wang X, Alam M, Sanjayan J, Wilson J. Parametric analysis for performance enhancement of phase change materials in naturally ventilated buildings. Energy Build. 2016;124:35–45.
203. Guarino F, Athienitis A, Cellura M, Bastien D. PCM thermal storage design in buildings: experimental studies and applications to solaria in cold climates. Appl Energy. 2017;185:95–106.
204. Jin Q, Long X, Liang R. Numerical analysis on the thermal performance of PCM-integrated thermochromic glazing systems. Energy Build. 2022;257: 111734.
205. Gowreesunker B, Stankovic S, Tassou S, Kyriacou P. Experimental and numerical investigations of the optical and thermal aspects of a PCM-glazed unit. Energy Build. 2013;61:239–49.